

American Journal of Science

MARCH 1994

A SYMMETRY-BASED METHOD FOR KINEMATIC ANALYSIS OF LARGE-SLIP BRITTLE FAULT ZONES

DARREL S. COWAN* and MARK T. BRANDON**

ABSTRACT. We apply a symmetry-based, statistical method for kinematic analysis of mesoscale fault-zone structures to resolve the transport directions for the Rosario fault zone and Lopez Structural Complex in the San Juan Islands. Both moderately dipping fault zones accommodated large amounts of Late Cretaceous slip (> 30 km), but the transport direction of nappes overlying these fault zones is controversial. Individual asymmetric folds and Riedel composite structures consisting of arrays of fault-related planar shear fractures and foliations are represented by an internal rotation axis, which describes the sense of shear and orientation of each structure. Synoptic stereographic analyses show that the internal rotation axes lie in a plane parallel to the fault zone but are widely dispersed within it. The fault-parallel distribution of internal rotation axes has a Gaussian form, centered around a mean direction.

We propose that the mean of the distribution reflects a deterministic process, the monoclinic symmetry of progressive deformation in an idealized, non-coaxial shear zone, and that stochastic and antecedent processes result in random variations about the mean. Therefore, the circular mean of the distribution is used to define a synoptic internal rotation axis, which according to the model should lie normal to the mirror plane of symmetry for the deformation and hence normal to the average slip vector for the fault zone. The symmetric Gaussian dispersions of internal rotation axes in the Lopez and Rosario fault zones are hypothesized to have resulted from processes such as local perturbations in the orientation of layering with respect to the slip direction or shear plane or rotations about fault-normal axes.

Slip vectors derived from synoptic analyses of mesoscale folds are top-to-the-south for the Lopez fault zone and top-to-the-southwest for the Rosario zone. Riedel structures in the Rosario fault zone formed within two conjugate sets of localized shear zones; slip on one set was top-to-the-northwest and on the other, top-to-the-southeast. The internal rotation axes for the Riedel structures have a bimodal distribution and inferred orthorhombic symmetry indicating bulk northeast-southwest shortening normal to the Rosario zone. The overall deformation in the zone is interpreted as a general non-coaxial shear with monoclinic symmetry.

* Department of Geological Sciences, University of Washington, Seattle, Washington 98195.

** Department of Geology and Geophysics, Yale University, New Haven, Connecticut 06511.

A post-faulting, solution-mass-transfer cleavage superimposed on the fault zones and nappes alike also records bulk shortening in a northeast-southwest direction. These compatible results support the hypothesis that the San Juan thrusts and nappes, and the larger Cascade orogen encompassing them, developed during northeast-southwest regional shortening in Late Cretaceous time.

INTRODUCTION

Kinematic analyses of micro- and mesoscale structures in ductile shear zones and brittle fault zones are used to interpret the relative transport direction of the blocks that bound the zones. For ductile and mylonitic shear zones dominated by crystal-plastic deformation mechanisms, published studies of kinematic indicators, such as composite foliations and rotated porphyroclasts, are commonplace. In contrast, large-slip brittle fault zones, which are characterized by distributed faults and cataclastic shear zones, have received less attention, even though they are widespread in orogenic belts, such as the western Cordillera of North America.

The purpose of this paper is to present a symmetry-based method for analyzing the kinematics of mesoscale structures in brittle fault zones. The method is based on the premise that the monoclinic symmetry of an idealized non-coaxial shear zone may be recorded in the fabric of the fault zone. The fabric is determined not only by the symmetry of the deformation but also by the symmetry of processes preceding and attending deformation. These ancillary processes may introduce random variation to the fabric distribution and hence contribute to the "messiness" of the data in a way that does not strictly accord with the predictions of deterministic models. Our symmetry-based method of analysis allows us to isolate, with a minimum number of assumptions, only that information needed to deduce the average direction of slip for a fault zone.

We apply our method to two Late Cretaceous, large-slip (> 30 km) brittle fault zones in the San Juan Islands of western Washington State (figs. 1 and 2). First, we review the setting of these fault zones and the controversy regarding the transport direction of nappes juxtaposed along them. Next, we review the symmetry principles and then develop a method for statistically analyzing the orientation distributions of asymmetric folds and Riedel structures. Finally, we use the symmetry of these fault-related fabrics to deduce the slip vectors for the Rosario and Lopez fault zones.

GEOLOGIC OVERVIEW OF THE CASCADE OROGEN

The Cascade orogen lies at the southern end of a 1200 km-long intra-Cretaceous orogenic belt extending from northwestern Washington and southwestern British Columbia to southeastern Alaska (Rubin and others, 1990) (fig. 1). At about latitude 49°N, the orogen can be divided into four generally northwest-striking tectonic zones (fig. 2). The westernmost zone consists of lower Paleozoic to Middle Jurassic rocks of Wrangellia, which is part of the larger Insular superterrane. Wrangellia

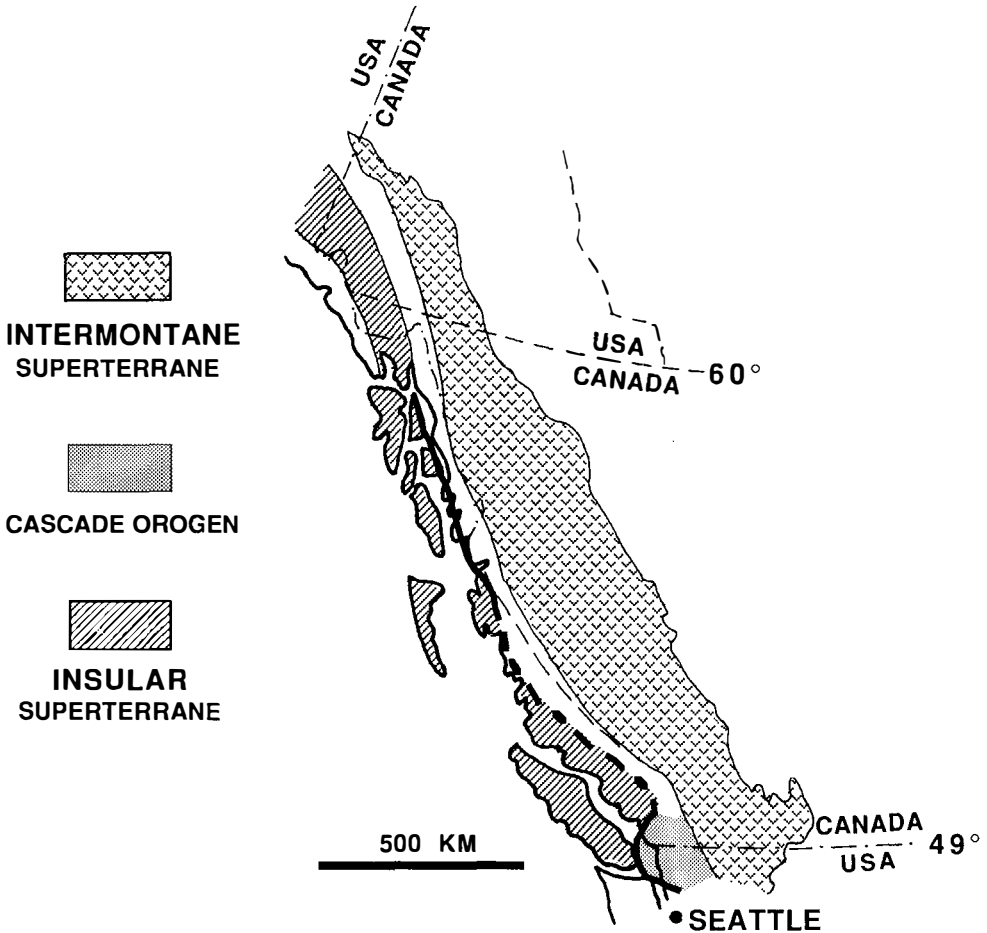


Fig. 1. The Cascade orogen lies at the southern end of a zone of mid-Cretaceous deformation (Rubin and others, 1990) at the eastern edge of the Insular superterrane. The heavy line denotes the approximate western boundary of the zone.

is unconformably overlain by the Nanaimo Group, a synorogenic basal sequence that formed adjacent to and received detritus from the San Juan-Cascade nappes. Inboard of Wrangellia is the San Juan-Cascade thrust system, composed of Late Cretaceous thrust faults and nappes of the San Juan Islands and northwest Cascades; this system developed mainly during the interval 100 to 84 Ma (Misch, 1966; Brandon, Cowan, and Vance, 1988; Brandon, 1989). The nappes within this zone were derived from a diverse assemblage of older terranes ranging in age from early Paleozoic to latest Early Cretaceous. The system as a whole appears to overlie structurally the more outboard Wrangellia terrane (Palumbo

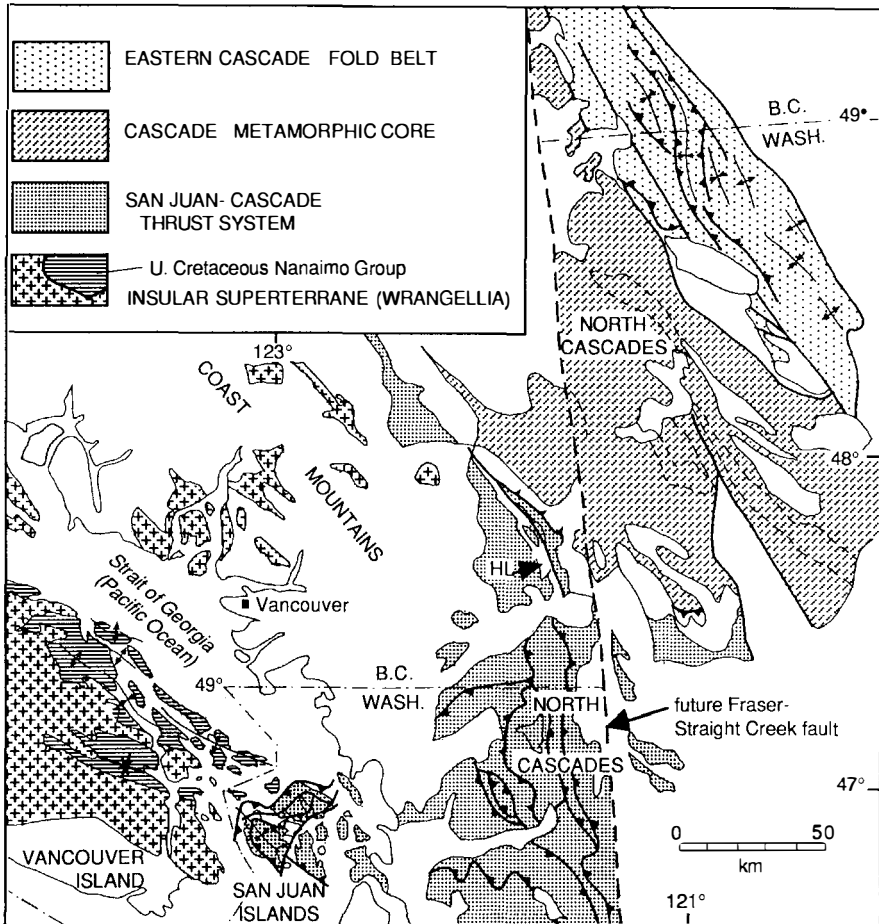


Fig. 2. Simplified regional map illustrating major Cretaceous tectonic elements in the Cascade orogen in northwestern Washington and southwestern British Columbia (see text for details). The palinspastic base (note offset of 49°N parallel) restores about 180 km of early Tertiary dextral slip on the Fraser-Straight Creek fault (after Misch, 1977; Brandon, 1989). Heavy lines with barbs represent Late Cretaceous thrust faults (barbs on upper plates). Undecorated heavy lines mark early Tertiary high-angle faults. Hinge lines mark Late Cretaceous and early Tertiary folds in the eastern Cascade foldbelt and Nanaimo Group, respectively. The northwest structural trend of the Cascade metamorphic core is highlighted by dashed lines which show the margins of deformed Cretaceous granitoid plutons. Unpatterned areas on land correspond to post-tectonic units, including Late Cretaceous and Tertiary plutons, or Cenozoic sedimentary and volcanic deposits. HL = Harrison Lake. Map compiled from figures in Monger (1986, 1990), England and Calon (1991), Brandon (1989), Brown and Talbot (1989), McGroder (1989, 1991), and Haugerud and others (1991).

and Brandon, 1990). The next zone to the northeast, the Cascade metamorphic core, was affected by high-temperature metamorphism, crustal thickening, and plutonism during the Late Cretaceous and early Tertiary (Misch, 1966; Babcock and Misch, 1988; Haugerud and others, 1991; Miller and others, 1993). The easternmost zone is the eastern Cascade fold belt (McGroder, 1989), consisting of a faulted and folded sequence of Triassic to Lower Cretaceous (Cenomanian) sedimentary and volcanic rocks. Deformation there occurred mainly between 100 and 88 Ma.

The relationship among these elements, and particularly between the San Juan-Cascade thrust system and the metamorphic core, is currently controversial. Although all workers agree that Cretaceous faulting played an important role in fashioning the structure of this belt, there has been considerable disagreement about the orogenic displacements within it. The *contraction model* (fig. 3A), advocated originally by Misch (1966) and subsequently by Brandon and Cowan (1985), Brandon, Cowan, and Vance (1988), Brandon (1989), McGroder (1991), and Journeay and Friedman (1993), postulates that the entire orogen formed by large-scale, southwest-northeast contraction which drove the San Juan-Cascade nappes over (Brandon and Cowan) or out of (McGroder; Journeay) the metamorphic core and onto the adjacent Wrangellia terrane. The implied transport direction of the nappes would have been dominantly top-to-the-southwest. Orogenic contraction is attributed to the collision of Wrangellia against North America (Davis, Monger, and Burchfiel, 1978; Monger, Price, and Tempelman-Kluit, 1982). The contraction model accounts for the large amount of orogenic shortening recorded by the San Juan-Cascade thrust system, probably on the order of 200 to 400 km (Brandon, 1989; McGroder, 1991).

An alternative model (fig. 3B), advocated by Brown (1987), Smith (1988), Brown and Talbot (1989), and Maekawa and Brown (1991), proposes that the San Juan-Cascade nappes developed in a generally northwest-striking transcurrent shear zone and that the nappes were driven to the northwest onto a Wrangellia terrane that had already been accreted to North America. This model, which we refer to as the *transcurrent model*, implies a transform boundary to the east, separating the northwest-moving nappes from a fixed North America. This boundary might correspond to the Cascade metamorphic core, which Brown and Talbot (1989) interpreted as a broad, right-lateral shear zone.

A critical difference between the contraction and transcurrent models is the predicted direction of fault slip within the San Juan-Cascade system. The contraction model requires that slip between the nappes was dominantly top-to-the-southwest. The transcurrent model emphasizes dextral slip on high-angle faults and shear zones throughout the Cascade orogen. Proponents of the transcurrent model have conceded that there are thrust faults present in the San Juan-Cascade system, but they consider these to be local features associated with left-stepping jogs within a wide system of dextral transcurrent faults (Maekawa and Brown,

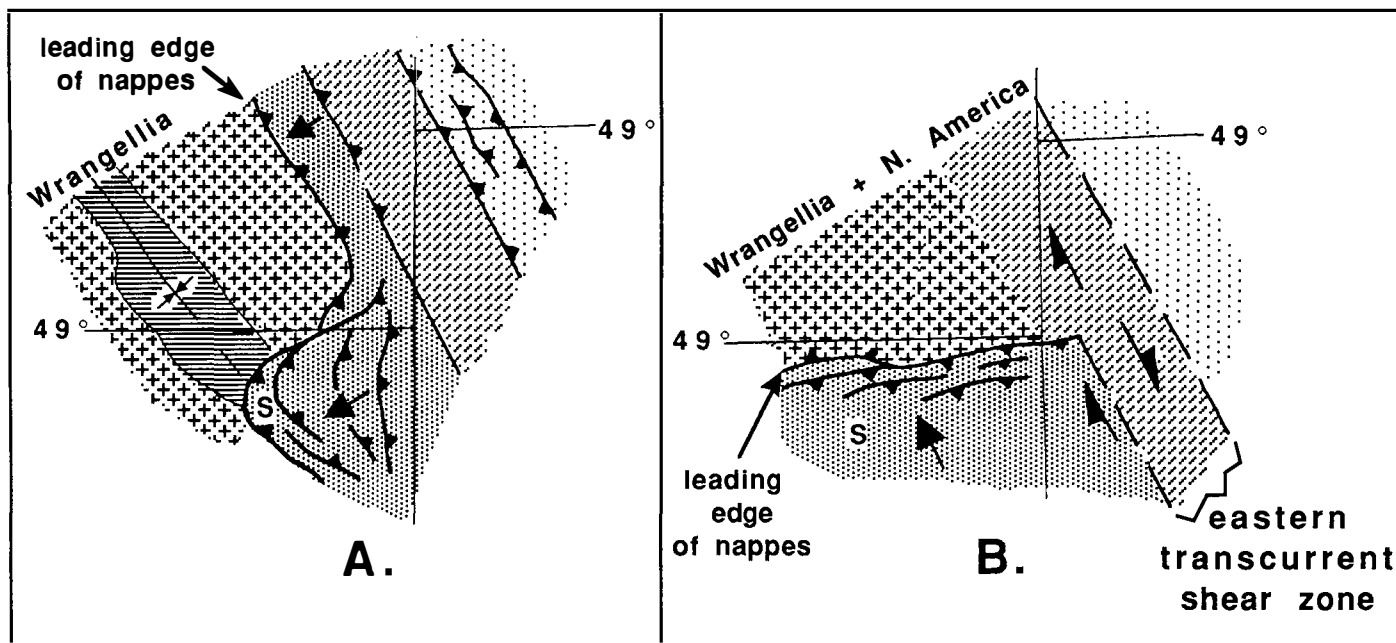


Fig. 3. Schematic maps depicting contrasting interpretations of the Late Cretaceous Cascade orogen. Large arrows indicate directions of relative transport. The future trace of the Fraser-Straight Creek fault and the 49°N parallel offset along it are provided for reference (see fig. 1). Patterns for units are the same as those in figure 1. S represents location of San Juan Islands (study area). (A) In the contraction model (Brandon and Cowan, 1985; McGroder, 1991), the Cascade orogen formed by northeast-southwest contraction associated with collision of Wrangellia. The San Juan-Cascade nappes are inferred to have been transported predominantly to the southwest and west, with respect to a fixed footwall, Wrangellia. The Nanaimo Group is interpreted to have formed as a foreland basin in front of the advancing nappes. (B) In the transcurrent model (Brown, 1987; Brown and Talbot, 1989; Maekawa and Brown, 1991), the Cascade orogen marks the trace of a major northwest-southeast transcurrent shear zone. In particular, the Cascade metamorphic core is considered to be a broad ductile shear zone (Brown and Talbot, 1989) which separates a north-moving assemblage of allochthonous terranes from a relatively fixed continental interior to the east. Thrust faults in the San Juan Islands have been interpreted by Maekawa and Brown (1991) as marking a system of "step-over" faults which transferred lateral slip from the Cascade core to the west side of Wrangellia. If correct, the San Juan thrusts should have a slip direction of top-to-the-northwest.

1991). In the transcurrent model, displacements on thrust faults should be top-to-the-northwest.

NAPPES AND LARGE-SLIP THRUST FAULTS IN THE SAN JUAN ISLANDS

Over the last 15 yrs, the geology of the San Juan Islands has been scrutinized by several research groups. Detailed field mapping and extensive paleontological and isotopic dating have yielded a fairly complete understanding of the general geology of the area. Available information was compiled and synthesized by Brandon, Cowan, and Vance (1988) and Brandon (1989); these sources provide the primary basis for the following summary.

The geology is characterized by a stacked sequence of thrust nappes (fig. 4). Each nappe is dominated by a stratigraphically related group of

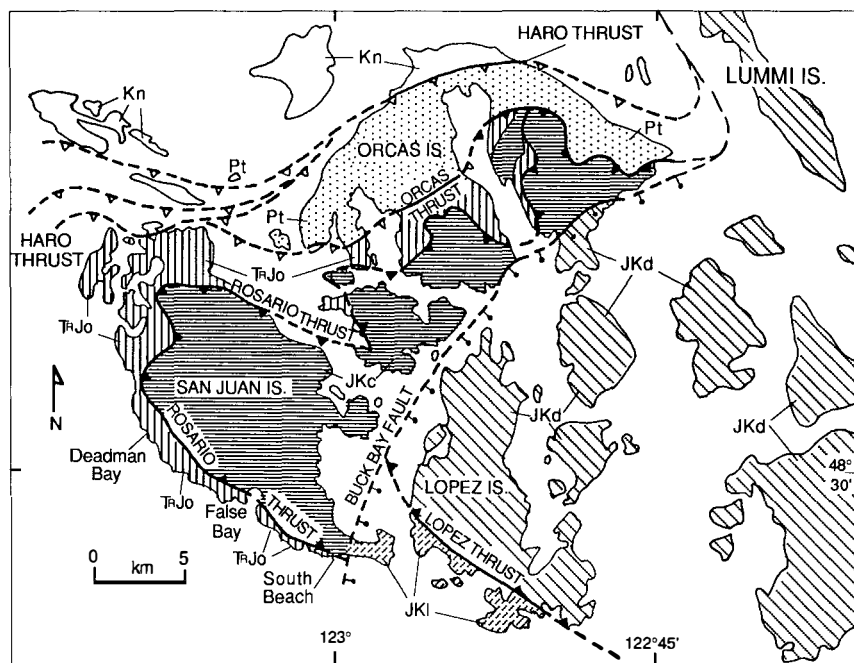


Fig. 4. Generalized geology of part of the San Juan Islands showing the major large-slip thrusts: Haro, Orcas, Rosario, and Lopez. JKd = rocks of the Decatur terrane, constituting the upper plate of the Lopez thrust. JKl = Lopez Structural Complex composed of diverse imbricated slices within the Lopez fault zone. JkC = Constitution Formation, a nappe bounded above by the Lopez Structural Complex and below by the Rosario thrust. TRJo = predominantly Triassic-Jurassic Orcas Chert of the Deadman Bay terrane which underlies the Rosario thrust. Within the Rosario thrust zone, the Orcas Chert is characterized by pervasive imbrication and brittle shear-related mesoscale structures. Pt = Paleozoic Turtleback Complex and related rocks. Kn = Upper Cretaceous Nanaimo Group. The Buck Bay fault inferentially dips southeast and is interpreted by Brandon (1989) to be a minor normal fault. Map adapted from figures 3 and 5 in Brandon, Cowan, and Vance (1988).

rock units. At present, the nappes are shaped into broad folds that trend and plunge gently to the southeast and have wavelengths of about 12 km. These folds are inferred to be early Tertiary in age because they are similar both in style and orientation to folds in the Upper Cretaceous Nanaimo Group and the Eocene Chuckanut Group exposed on the mainland east of the San Juan Islands (England and Calon, 1991).

Because the faults at the boundaries of the thrust nappes juxtapose unrelated tectonostratigraphic units, we conclude that they have accommodated large amounts of slip, probably in excess of tens of kilometers (see below for specific estimates). Within the nappes, there is evidence for local imbrication and faulting, but the slip on these internal structures must be relatively minor because stratigraphic offsets are small or not apparent. On this basis, we distinguish between large-slip faults, which commonly form the major terrane-bounding structures, and small-slip faults, which offset or imbricate a given rock unit but do not juxtapose unrelated terranes.

Four large-slip faults have been recognized in the San Juan Islands: the Haro, Orcas, Rosario, and Lopez thrusts (fig. 4). Of these, the Rosario and Lopez thrusts are exceptionally well exposed in wavecut outcrops along the southwestern coasts of San Juan and Lopez islands. Our study here has focused specifically on these outcrops. Brandon, Cowan, and Vance (1988) provide detailed maps of each of these fault zones.

Rosario Fault Zone

The Rosario fault zone (fig. 4) has a sinuous trace that extends about 65 km across the San Juan Islands. The hangingwall consists of the upper Mesozoic Constitution Formation, an interbedded sequence of volcanoclastic sandstone, mudstone, and minor ribbon chert and pillow basalt. The footwall is composed of the Lower Permian to Middle Jurassic Deadman Bay terrane, composed mainly of ribbon chert with subordinate pillow basalt and limestone. In our mapping, we have identified a specific fault surface, the Rosario thrust (fig. 4), which corresponds to the upper limit of Deadman Bay rocks and also marks the top of an intensely faulted zone which varies in thickness from about 200 to 1000 m. This zone is dominated by meter-, decimeter-, and kilometer-scale slices of ribbon chert and minor pillow basalt of the Deadman Bay terrane. Slices of other units, unrelated to the subjacent Deadman Bay terrane, are typically restricted to the uppermost part of the fault zone. For instance, slices of Constitution Formation are generally confined to the uppermost 10 m of the zone. Dispersed within the upper 100 to 200 m of the fault zone are exotic meter- to decimeter-size slices of Garrison Schist, which includes mafic and quartzose schists metamorphosed to greenschist- and albite-epidote amphibolite facies. Several K-Ar amphibole dates indicate a Permian and/or Triassic age for this metamorphism. The rocks within the fault zone, as well as the nappes above and below, record a regional high pressure-low temperature metamorphism characterized by widespread prehnite and aragonite, with minor lawsonite and pumpellyite.

The slices of Garrison Schist are found along much of the mapped extent of the Rosario fault (figs. 3 and 13 in Brandon, Cowan, and Vance, 1988). These slices must represent an exotic component, because they cannot be related to the present footwall or hangingwall of the Rosario fault zone. In other words, we cannot find a footwall or hangingwall cutoff from which the slices of Garrison might have been derived. Likewise, there is no apparent footwall cutoff from which the Constitution Formation in the overlying nappe was derived. Both these relationships indicate that offset on the Rosario fault zone must exceed the present amount of structural overlap across the zone. This overlap requires a minimum of 30 km of slip for a top-to-the-southwest direction and 18 km for a top-to-the-northwest direction. The presence of the Garrison slices in the upper part of the zone suggests that much of this estimated minimum slip must have been accommodated in the upper 100 to 200 m of the fault zone. Thus, we consider the Rosario thrust and the uppermost part of the Rosario fault zone to mark the locus of a large-slip fault. Most of the distinctive fault-zone structures described herein are in this part of the Rosario fault zone.

Lopez Structural Complex

The Lopez Structural Complex (fig. 4) is a 3-km thick, northeast-dipping fault zone lying beneath the Lopez thrust. The hangingwall is a relatively coherent nappe, the Decatur terrane, which encompasses the Fidalgo Igneous Complex, a Middle and Upper Jurassic ophiolite and volcanic arc, and overlying Upper Jurassic marine clastic strata of the Lummi Group. The footwall is the Constitution Formation. The Lopez Complex consists of imbricated lenticular slices that were mostly derived from adjacent hangingwall and footwall units. However, two exotic units are present. Lower Paleozoic tonalite and gabbro are found in two small (<150 m) fault slices. These rocks are equivalent to the Turtleback Igneous Complex which is mainly exposed in the northern San Juan Islands (20 km north of the Lopez Complex), where it forms one of the lowest nappes in the stack. Small fault slices of Turtleback Complex are distributed locally in other fault zones of the San Juan Islands (fig. 3 in Brandon, Cowan, and Vance, 1988), but the slices in the Lopez Complex represent the structurally highest occurrence of this unit. The other exotic unit consists of the uppermost Albian pillow basalts of Richardson, which is restricted to a 3 km-long slice in the Lopez Complex. Like the Garrison slices in the Rosario fault zone, we cannot find a footwall or hangingwall cutoff from which the basalts of Richardson might have been derived.

The minimum amount of slip across the Lopez fault zone can be estimated by considering the minimum distances required to restore the hangingwall and exotic fault slices back to their footwall sources. For the case of top-to-the-southwest transport, the nearest footwall source for the Turtleback Complex (easternmost tip of Orcas Island) indicates a minimum slip of 26 km. The absence of a footwall source for the basalts of

Richardson gives a similar minimum estimate. These relationships cannot be used for the case of top-to-the-northwest transport because the Lopez zone lies at the southern outcrop limit of the San Juan nappes. The absence of a pronounced gravity anomaly over the Decatur terrane indicates that much of the mantle base of this ophiolitic nappe is probably missing. This relationship implies that the amount of slip on the Lopez fault must be greater than the dimensions of the Decatur nappe itself. This argument indicates a minimum slip of about 30 km, regardless of transport direction, because of the equant shape in map view of the Decatur terrane (fig. 3 in Brandon, Cowan, and Vance, 1988).

To summarize, the Lopez and Rosario fault zones are similar in two respects: (1) they both have accommodated large amounts of fault slip (>30 km), and (2) they both contain exotic fault slices. There are some important contrasts. For the Lopez Complex, (1) the fault zone is much thicker (3 km versus ~200 m), (2) fault slices of different parentage (that is, hangingwall, footwall, or exotic sources) appear to be more evenly distributed within the zone, and (3) fault-related deformation appears to be less intense. These observations suggest that slip across the Lopez Complex was accommodated on a more evenly distributed system of faults, whereas slip across the Rosario zone was strongly localized at the top of the zone.

Deformational and Metamorphic History of the Rosario and Lopez Fault Zones

Brandon, Cowan, and Vance (1988) and Brandon, Cowan, and Feehan (1993) presented evidence for a well-defined sequence of deformation, metamorphism, and uplift between about 100 and 84 Ma in the San Juan Islands. The earliest event in this Late Cretaceous history was the juxtaposition of nappes along the Rosario, Lopez, and kindred large-slip fault zones (fig. 4). This event is interpreted as no older than 100 Ma, on the basis of the latest Albian age of the youngest rocks included in the Lopez Complex. The imbrication of fault slices and the transport of exotic blocks within these fault zones occurred in a deformational regime dominated by brittle microfracturing and cataclastic flow.

The entire thrust system, including nappes and fault zones, was subsequently affected by a very low-temperature, high-pressure metamorphism, recorded by the static growth of lawsonite, pumpellyite, prehnite, and aragonite. Supporting petrographic observations are in Brandon (1980), Brandon, Cowan, and Vance (1988), and Brandon, Cowan, and Feehan (1993). Here, we emphasize metamorphic textures in the exotic fault slices of Garrison Schist and Turtleback Complex because they provide the clearest evidence of the relative timing of metamorphism and faulting (fig. 5). The relatively undeformed veins of aragonite and lawsonite commonly overprint a pervasive cataclastic fabric found in most of the exotic fault slices (fig. 5A and B). This fabric is attributed to brittle deformation associated with the incorporation and transport of these blocks in the fault zones. We conclude that metamorphism must have postdated much, if not all, of the slip within these fault zones. Note

that our conclusions differ from those of Maekawa and Brown (1991, 1993), who argued that metamorphism is synchronous with faulting. Metamorphic assemblages, together with apatite and zircon fission-track ages, indicate that peak metamorphic conditions for the Rosario and Lopez zones and adjacent nappes were in the range of 150° to 200°C and about 500 Mpa (5 kb).

After imbrication and peak metamorphism, a prominent solution-mass-transfer cleavage was locally formed. This cleavage is best developed on southern San Juan Island, southern Lopez Island, and Lummi Island (fig. 4). In all cases, it dips moderately to the northeast (fig. 6). In thin section, the cleavage is defined by dark discontinuous selvages with a spacing of 1 to 5 mm. Detrital grains in sandstone commonly show overgrowths of straight fibers oriented parallel to the cleavage. These fibers mark the extension direction during cleavage formation. Where best studied in the southern San Juan Islands, the cleavage appears to postdate fault-zone deformation and high-pressure metamorphism in the Rosario and Lopez fault zones. For example, in many cases, the cleavage can be traced across specific faults or from fault slices into a surrounding fault-zone matrix. Furthermore, we have found veins of lawsonite + quartz that were shortened or extended depending on their initial orientation to the principal directions of cleavage-related strain (fig. 5C and D).

Maekawa and Brown (1991, 1993) argued that this cleavage was formed by non-coaxial shear associated with fault slip. We disagree. Our observations indicate that the cleavage is a widespread regional feature and is not confined to individual fault zones. Furthermore, the straight fibers associated with the cleavage indicate that cleavage-related deformation was coaxial. We interpret this cleavage to have formed by late-stage ductile shortening within the thrust wedge after accretion of the nappes.

We conclude that the high-pressure metamorphism and subsequent development of cleavage are regional-scale events which occurred before 84 Ma. The best evidence for timing is a Santonian conglomerate in the Upper Cretaceous Nanaimo Group (figs. 1 and 4) that contains cobbles of lawsonite-bearing sandstone closely resembling the metamorphosed Constitution Formation. Apatite fission-track ages from the San Juan Islands, indicating cooling at ~87 Ma (Johnson and others, 1986; Brandon, Cowan, and Vance, 1988), are compatible with the interpretation that the nappes were uplifted and erosionally unroofed to supply detritus to the Nanaimo Group.

In summary, the orogenic history of the San Juan nappes consisted of: (1) juxtaposition of nappes along large-slip Rosario, Lopez, and related fault zones; (2) attendant brittle fault-zone deformation; (3) metamorphism; (4) formation of cleavage; and (5) erosional exhumation. All these events took place within a 16 my interval (100-84 Ma), during which the nappes traversed a round-trip vertical distance of about 36 km, at an average vertical rate of about 2 km/my. Brandon, Cowan, and Vance (1988, fig. 29) favor the interpretation that high-pressure metamorphism

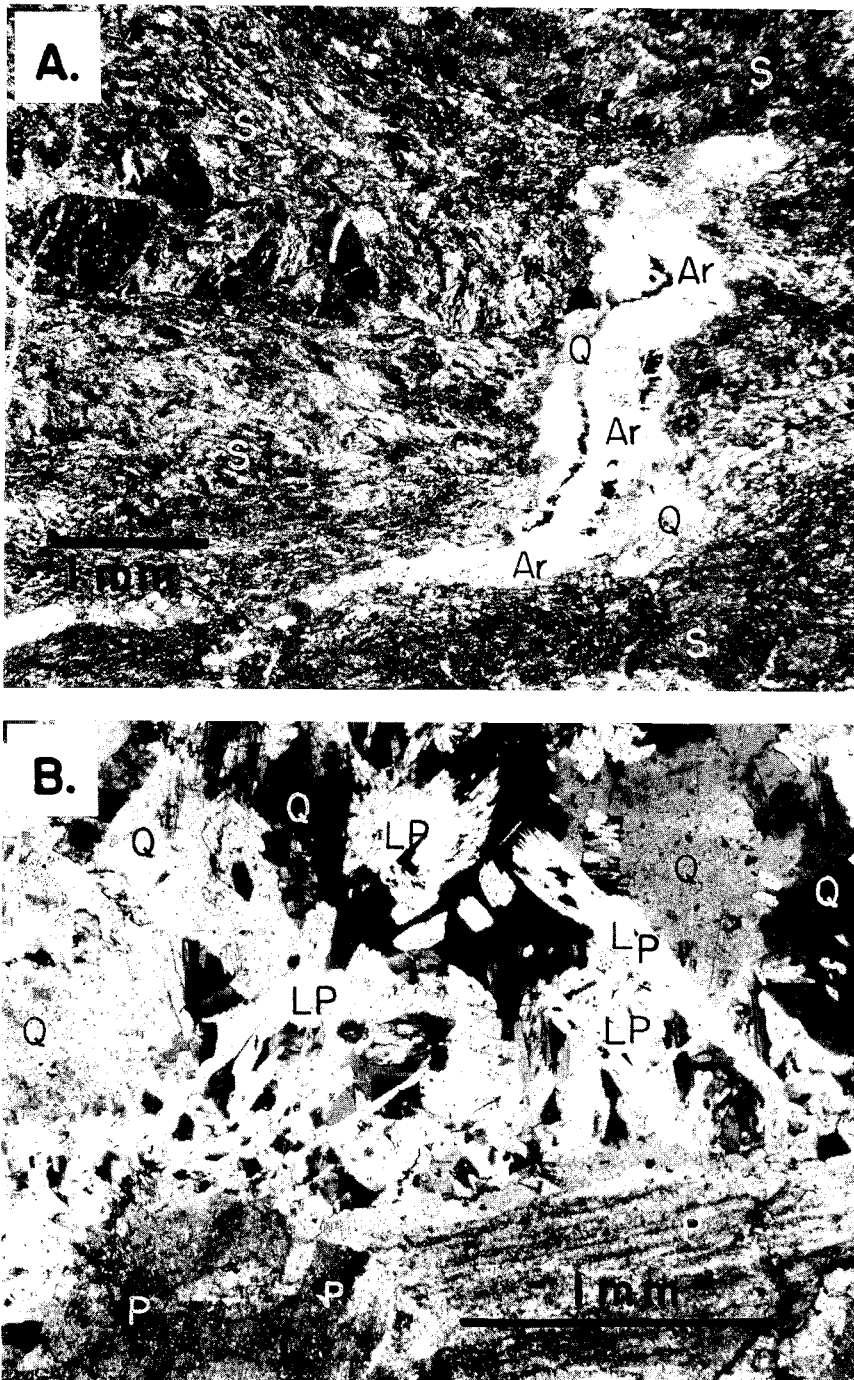


Fig. 5. Photomicrographs illustrating timing relationships between fault-zone deformation, metamorphism, and cleavage formation. (A) Strongly cataclastic actinolite-chlorite schist, from an exotic fault slice of Garrison Schist located in the Rosario fault zone 2 km northwest of South Beach, southern San Juan Island. The schist (S) is cut by a relatively undeformed vein of aragonite (Ar) and minor quartz (Q), which formed during high pressure metamorphism. The aragonite is variably retrograded to calcite. (B) Strongly cataclastic tonalite, from an exotic fault slice of Turtleback Complex located in the Lopez Complex at Cape San Juan, southern San Juan Island. Quartz (Q) and plagioclase (P) of the original tonalite were cataclased during emplacement of the slice into the Lopez Complex. Radiating blades of undeformed lawsonite + pumpellyite (LP) indicate that high-pressure metamorphism postdated cataclasis.

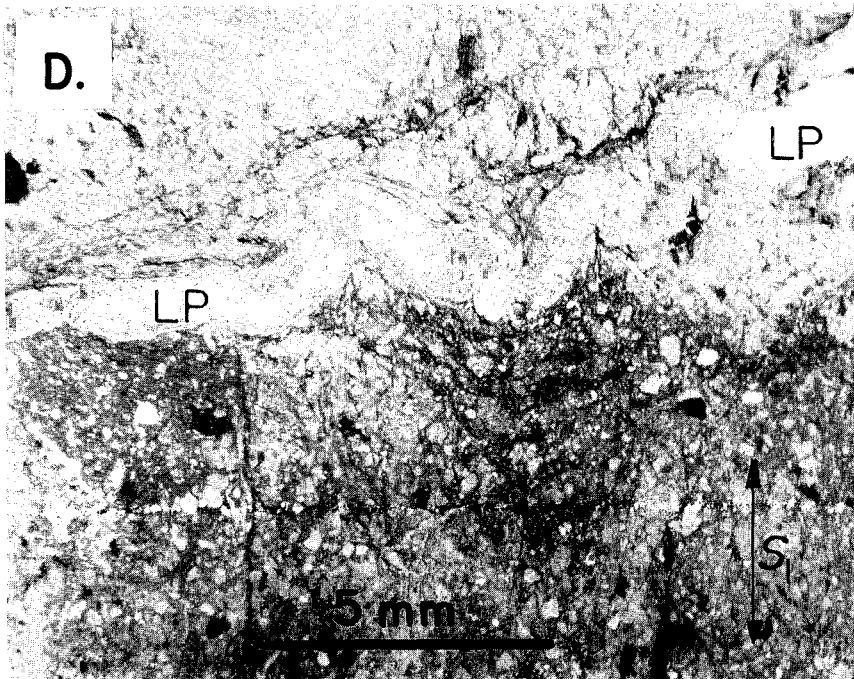
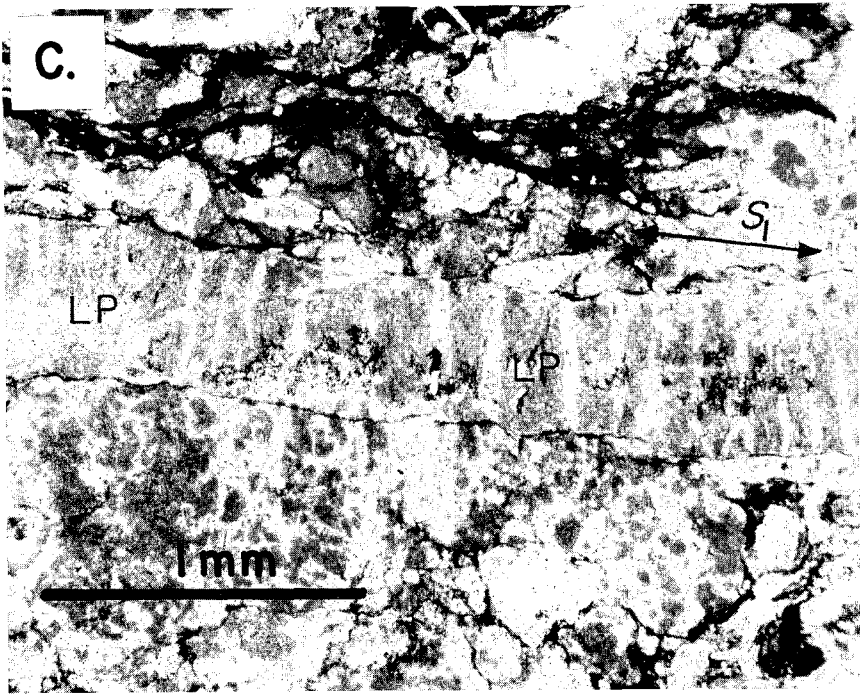


Fig. 5(C) Sands one with a pulled-apart vein of lawsonite and pumpellyite (LP) oriented parallel to the trace of the solution-mass-transfer cleavage (S_1). The extensional openings between boudin fragments are filled with fibrous quartz and minor CaCO_3 . The vein is inferred to have been extended during cleavage formation. This sample is from a slice of Constitution Formation in the Lopez Complex on the southern tip of San Juan Island. (D) Sandstone with a lawsonite + pumpellyite vein (LP) that was shortened and folded during cleavage formation. S_1 marks the trace of cleavage. Sample is from the same locality as that described in the previous photomicrograph.

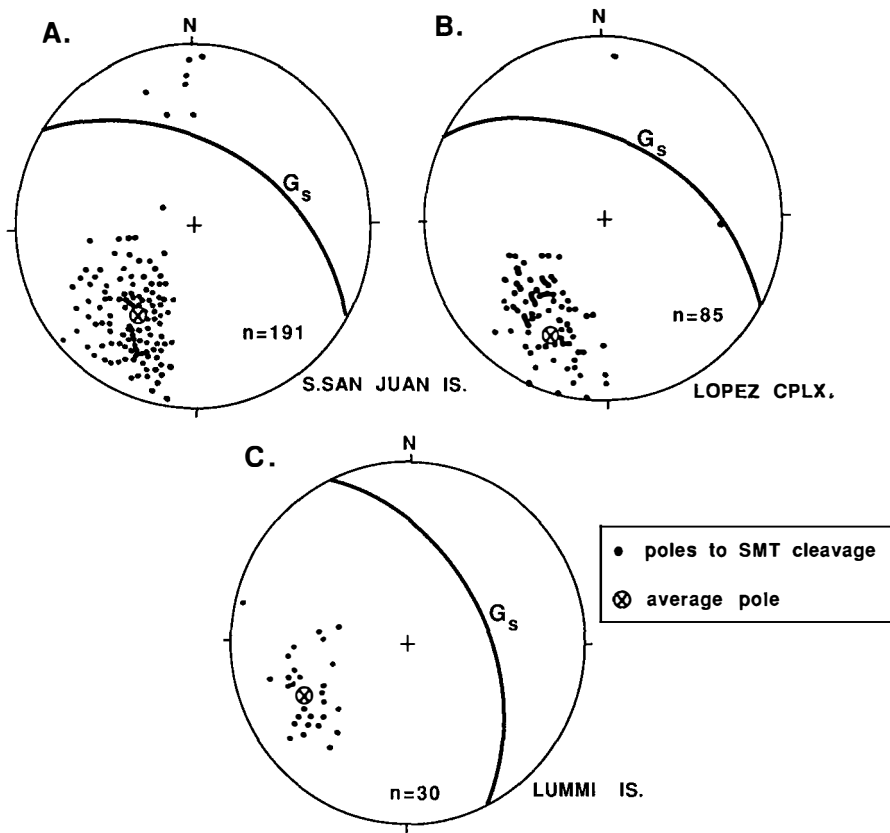


Fig. 6. Lower hemisphere, equal-area stereograms of poles to the solution-mass-transfer cleavage. The great circle, labelled G_s , marks the average attitude of the cleavage, and the large crossed circle, its pole. (A) Constitution Formation, Lopez Complex, and Orcas Chert on southern San Juan Island (Brandon, 1980). Average attitude of G_s is 121° , 53° N. (B) Lopez Complex on southern Lopez Island (Cowan, unpublished mapping). Average attitude of G_s is 120° , 55° N. (C) Decatur terrane on Lummi Island (Carroll, 1980). Average attitude of G_s is 154° , 54° E.

was caused by accretion of the San Juan nappes at a depth of about 18 km beneath an actively advancing orogenic wedge.

In view of this well-established history, we feel that the San Juan thrust system provides an excellent opportunity to examine mesoscale structures formed within deeply seated brittle fault zones. We are reasonably confident that the fault zones have accommodated large slip, on the order of 30 km. What remains controversial and poorly resolved is the direction of slip.

KINEMATIC ANALYSIS OF BRITTLE FAULT ZONES

A primary goal of kinematic analysis of brittle fault zones and ductile shear zones is to estimate the average direction of relative transport at the

regional scale. Analysis typically involves studying meso- or microscale structures and fabric elements to infer the sense-of-shear, the slip directions, and, in some cases, the direction of maximum extension. Most studies of the brittle regime, where low-temperature (<200°C) deformation involves dominantly frictional mechanisms, have emphasized wear features, fibers, and secondary fractures associated with discrete fault surfaces (Hancock, 1985; Petit, 1987). Other methods are used to infer the principal axes of stress or strain using regional arrays of small-slip (< ~1 km) faults (Angelier, 1984; Krantz, 1988; Marrett and Allmendinger, 1990).

In contrast, there are comparatively few published synoptic analyses that have focused on large-slip brittle fault zones, the topic of this paper. As defined here, a *brittle fault zone* is a localized tabular domain consisting of a dense set of contemporaneous, subparallel faults and brittle shear zones. We use the term *brittle shear zone* for zones of fault-generated materials, such as gouge and cataclasite, that have deformed in a penetrative or mesoscopically ductile fashion by cataclastic flow. Examples of papers that have treated the fabrics or kinematics of cataclastically flowing materials in brittle shear zones are: Chester, Friedman, and Logan (1985), Chester and Logan (1987), Twiss and Gefell (1990), Twiss, Protzman, and Hurst (1991), and Tanaka (1992).

Mesoscale Structures Used for Kinematic Analyses

Brittle fault and shear zones display a variety of features that are, at least in theory, useful for kinematic analysis, including: linear structures such as striations or fibers, rotated porphyroclasts set in a gouge matrix, folds, and characteristic sets of fractures and foliations. The Rosario and Lopez fault zones are nearly devoid of striations, so for our study, we have focused on the orientation of asymmetric folds and composite arrays of planar structures, which are widespread and well exposed.

Asymmetric folds.—Geologists have long hypothesized that the asymmetry of individual folds or populations of folds is somehow related to the sense of shear in shear zones. For example, Hanmer and Passchier (1991, p. 64) claimed, “of all shear-sense indicators, the asymmetry of shear associated folds is perhaps the most venerable.” However, they and others have noted that the initiation and geometrical evolution of folds depend on many factors, such as the orientation of layering, the homogeneity of the displacement field within a shear zone, and whether layering behaves in a mechanically active or passive way during deformation. Therefore, only in unusual cases can the orientation of individual folds be confidently related to the average shear direction of the shear zone.

Hansen (1967, 1971) presented what is probably the most widely employed method for determining the sense and direction of shear using populations of asymmetric folds (fig. 7). He used folds in a tundra landslide to develop a symmetry-based analysis which he argued was generally applicable to flexural and flexural-slip folds that “. . . result . . . from the motion of one layer or body of material past another” (Hansen, 1967, p. 390)—in other words, “drag folds” formed in shear zones. Folds

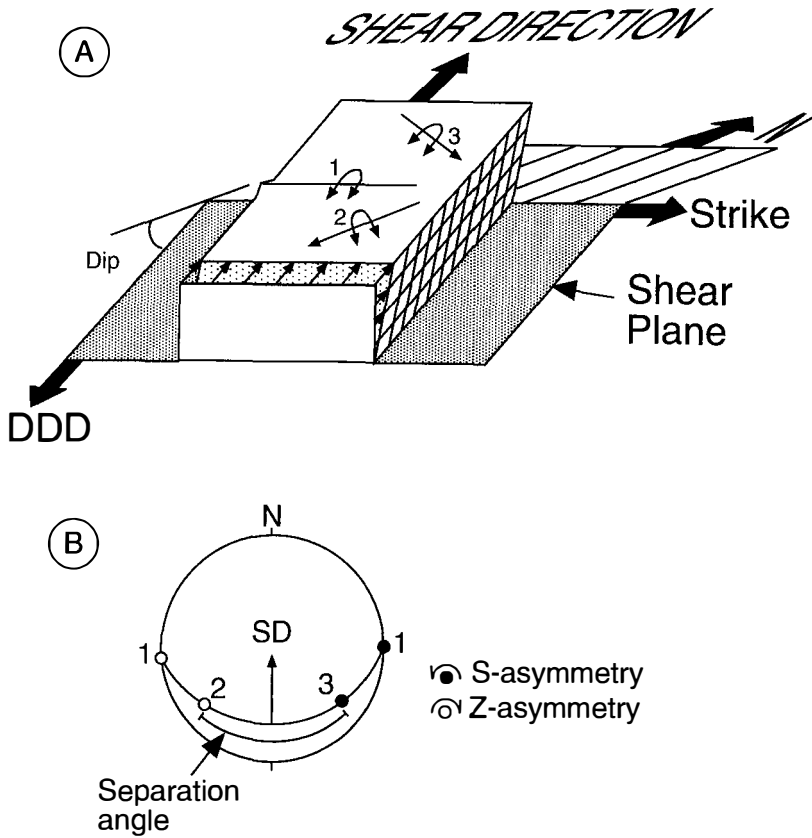


Fig. 7. Diagrams illustrating the relationship between asymmetric folds and the shear direction and how folds are analyzed kinematically according to the method of Hansen (1967, 1971). In (A), the material above the shear plane represents a mesoscopically ductile shear zone deformed by bulk progressive simple shear. Asymmetric folds that form in the shear zone will generally have hinge lines that lie parallel to the shear plane but may have a range of orientations within that plane. For example, the hinge line of fold #1 is normal to the shear direction, whereas the hinge lines of folds #2 and #3 are oblique. The strike and down-dip direction (DDD) of the shear plane are used as reference directions within the shear plane. In (B), the axis and sense of asymmetry of each fold are plotted on a lower hemisphere stereogram. By convention, the sense of asymmetry is assigned on the basis of the form of the fold when viewed in a down-plunge direction. The sense of asymmetry for fold #2 is clockwise, as indicated by the label "Z." The sense for fold #3 is anticlockwise, as indicated by the label "S." The down-plunge direction for fold #1 is ambiguous because its plunge is zero. In this case, the asymmetry is determined on the basis of the arbitrarily designated trend of the fold. For the stereogram, one should view the fold as if one were looking outward from the center of the stereogram. On this basis, fold #1 is assigned a "Z" sense-of-asymmetry when plotted with a westward trend and an "S" sense-of-asymmetry when plotted with an eastward trend. The fold axes define a girdle that parallels the orientation of the shear plane. Commonly, fold axes will plot as two distinct groups, with all Z folds in one group and all S folds in the other. The gap between these two groups is called the separation angle. According to the Hansen method, the shear direction (SD) for the shear zone (slip line in Hansen's terminology) is considered to lie within the separation angle. As used here, the shear direction is the direction of motion of the hangingwall relative to a fixed footwall.

in his tundra landslide developed initially with a wide range of orientations, but all fold hinges were nearly parallel to the slip surface at the base of the slide. Hence, in lower hemisphere stereographic projection, fold axes from the slide were co-planar and dispersed along a great-circle girdle (fig. 7). Hansen found that folds of opposite asymmetry or vergence plotted in two well-separated groups. He defined the angle between the groups as the separation angle and argued that the slip line, describing the net displacement of the folded mass with respect to its substrate, lay within the separation angle. The Hansen method has been applied to brittle fault and shear zones in fold-and-thrust belts (Stanley and Sarkisian, 1972; Wheeler, 1978) and subduction complexes (Moore and Wheeler, 1978; Platt, Leggett, and Alam, 1988), to slump folds (Woodcock, 1979), and to high-temperature shear zones (Carreras and Santanach, 1973; Coney, 1974). Woodcock (1979) and Platt, Leggett, and Alam (1988) also discussed statistical methods for analyzing the fold data.

Hansen's simple example of a tundra landslide illustrates the general principle that the hinge line of an individual fold need not be normal to the shear direction. However, the vergence of any given fold should be compatible with the overall sense of shear for the zone. What remains unclear is how to treat those situations where some folds have a vergence contrary to that expected for the general sense of shear, so that the groups of folds with opposite asymmetry overlap in stereograms. Hansen (1971, p. 51) made only a passing reference to this case and left the definition of the separation angle ambiguous. Furthermore, there are additional concerns as to the physical basis of the method and the circumstances that might limit its applicability. For example, is the method applicable in cases of general non-coaxial shear where there may be extension or shortening in the direction of transport? How does one detect the systematic biases that might be produced by pre-existing fabrics, such as layering oblique to the shear zone? In a section below, we use a symmetry argument (Paterson and Weiss, 1961) to develop a general physical rationale for Hansen's method. This rationale provides more complete guidelines for the application of the method and tests of its underlying assumptions.

Riedel structures.—A potentially useful, but largely untapped, kinematic resource is the suite of mesoscale shear fractures, foliations, and other planar fabrics that collectively result from non-coaxial deformation in brittle shear zones. We focus here on a distinctive set of planar structures (fig. 8) which have been recognized in experiments where shear zones are induced in soft clay and other simulated gouges (Morgens-tern and Tchalenko, 1967; Logan and others, 1979). We refer to this set as a *Riedel composite structure*, or *Riedel structure* for short, in the same sense that "composite structure" is used for the array of planar fabrics (S, C, and C') in mylonitic shear zones (Berthé, Choukroune, and Jegouzo, 1979). The relationship of Riedel structures to the geometry and shear direction of the shear zone has been well studied experimentally. These results show that a set of contemporaneous Y, P, and R structures is

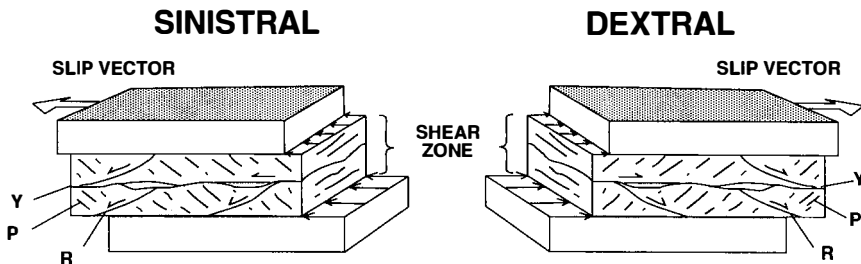


Fig. 8. Block diagrams showing the geometry of two idealized Riedel structures: one is sinistral (top-to-the-left), and the other dextral (top-to-the-right). The primary slip surface is labelled Y. Secondary additive faults, which are inclined in the direction of slip, are labelled R. Surfaces, including shear fractures or penetrative foliations, inclined in the opposite direction of slip are labelled P. In the Rosario fault zone, P is a cataclastic foliation, not a shear fracture.

developed (fig. 8) and that the overall symmetry of the structures is related to the monoclinic symmetry of the deformation.

Riedel structures have been observed in natural brittle shear zones at all scales. In principle, inspection of a Riedel structure in a section roughly normal to its shear and mirror planes should give a local estimate of the sense and direction of shear for the shear zone. However, an unresolved question is whether an individual Riedel structure in a natural fault zone will be representative of the bulk deformation in the fault zone at a regional scale. If not, it may be necessary to analyze a population of Riedel structures using a symmetry-based approach akin to the Hansen method for folds. While there is a growing informal utilization of Riedel structures to infer sense-of-shear in individual outcrops (Taira, Byrne, and Ashi, 1992), we know of only a few published studies (Rutter and others, 1986; Chester and Logan, 1987; Platt, Leggett, and Alam, 1988; and Kano, Nakaji, and Takeuchi, 1991) that have analyzed these structures at a regional scale.

A Symmetry-Based Method for Kinematic Analysis

As discussed above, several different techniques have been used to analyze fault kinematics: (1) analysis of shear-sense indicators in brittle shear zones; (2) analysis of striae and fault-surface features on discrete faults, and (3) tensor-based methods that determine the principal axes of stress or strain associated with a system of faults. We maintain that all these approaches, whether acknowledged or not, ultimately rest on principles of symmetry (Paterson and Weiss, 1961). Our conclusion applies equally to tensor-based methods, because the tensors used to describe the deformation (that is, the displacement gradient tensor, stress tensor, et cetera) carry information about symmetry (Nye, 1985). Our premise is that the fabric of rocks deformed in brittle fault zones may record the symmetry elements of the deformation, which can then be

combined with information provided by sense-of-shear criteria to yield an estimate of the bulk slip direction.

The fundamental objective of a symmetry argument is to relate the symmetry of the processes to that of the products. By *processes* or, in the terminology of Paterson and Weiss (1961), contributing factors, we mean those physical properties and fields—such as the pre-existing structure of the rock and the displacement fields and stresses attending deformation—that collectively produce the final fabric of the deformed rock. The symmetry of a deformed rock, according to Paterson and Weiss (1961), is defined by those symmetry elements that are present, and equivalent both in type and orientation, in all subfabrics that make up the total fabric of the rock. In their words, “Symmetry elements not present in all subfabrics are not symmetry elements of the fabric, and so a fabric cannot have symmetry higher than that of any of its subfabrics” (p. 868). Likewise, the symmetry of the combined processes includes only those symmetry elements common to all the individual processes.

The principles that underlie a symmetry argument can be summarized using the following statements from Paterson and Weiss (1961):

1. “. . . the symmetry that is common to [the processes] cannot be higher than the symmetry of the observed fabric” (p. 880).
2. “. . . symmetry elements absent in the fabric must be absent in at least one of the [processes]” (p. 880).
3. “. . . the final fabric may possess symmetry elements that are absent in the initial fabric or the deformation” (p. 879).

We divide processes into three types. The first type is called *deterministic* and refers to the forces and displacements attending deformation. The second type is called *stochastic* and refers to processes associated with deformation that cause random variations in the final fabric. Stochastic processes will reduce the strength of any preferred orientation, but they will not reduce the symmetry of the final fabric. The third type is called *antecedent* and refers to processes that affected the rocks prior to deformation and may have produced pre-existing structures. The symmetry of the final fabric may be reduced, and the symmetry of the deformation obscured in cases where pre-existing structures do not have symmetry elements common to those of the deformation, either due to low symmetry or oblique orientation. An example would be a layering with a systematically oblique orientation with respect to the shear plane of a shear zone.

The stochastic and antecedent processes will both contribute to the “messiness” of the observed data. Therefore, it is essential that the quantity of the data and the size of the study area are both large enough to average random variations. Our method assumes that the observed fabric is statistically homogeneous at the scale of the study area (see Paterson and Weiss, 1961). If the fabric lacks homogeneity at this scale, the data may not reveal its full symmetry.

Our goal is to use the symmetry of the fabric of a fault zone, as represented by the structures it contains, to deduce the symmetry of the

overall deformation. First, we postulate an idealized fault zone (fig. 9) in which the progressive non-coaxial deformation has monoclinic symmetry. The deformation in the fault zone represents the deterministic process. In accord with the symmetry principles, we consider three cases that might result from this type of deformation: (1) *Monoclinic fabric (a single mirror plane)*. In this case, we use the intersection of the mirror plane and the shear plane, together with information from sense-of-shear criteria (for example, asymmetric folds, Riedel structures), to define the slip vector for the fault zone. (2) *Orthorhombic fabric (three orthogonal mirror planes)*. This case can arise because the final fabric may have symmetry elements in addition to those common to the processes (see symmetry principle #3 above). In this case, all we can deduce is that the mirror plane of the shear zone corresponds to one of the three mirror planes of the fabric. (3) *Triclinic fabric (a center of symmetry with no mirror plane)*. This case can occur when one of the processes (for example, pre-existing, obliquely oriented layering) lacks symmetry elements in common with those of the deformation (see symmetry principle #2 above). No record remains of the monoclinic symmetry of the shear zone.

Geometric representation of fault-zone structures.—We represent the orientation and asymmetry of each individual fold and Riedel structure

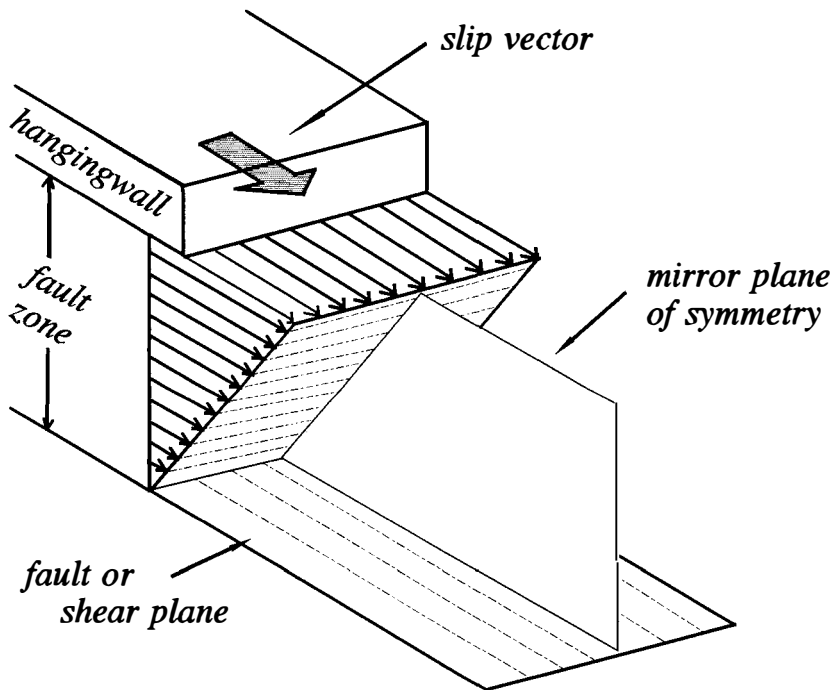


Fig. 9. Idealized fault zone illustrating the velocity distribution in a zone of progressive simple shear with monoclinic symmetry (adapted from fig. 1 in Twiss and Gefell, 1990).

with an *internal rotation axis* (fig. 10). This axis is similar to the internal vorticity vector of Means and others (1980) and Lister and Williams (1983); internal rotation corresponds to the total shear-induced rotation, and internal vorticity to the instantaneous shear-induced rotation. The term “kinematic rotation axis” used by David Elliott (S. Wojtal, personal communication, 1991) appears to be synonymous with our internal rotation axis, but it does not clearly distinguish the type of rotation involved (see Lister and Williams, 1983).

The internal rotation axis is not a normal polar vector but rather an axial vector for which we must designate a sense of rotation (Nye, 1985, p. 39). We use the geologic convention of designating the axis as either “S” or “Z” corresponding to an anticlockwise or clockwise rotation respectively, when viewed in the direction indicated by the vector. This convention makes it possible to display the internal rotation axes on a lower hemisphere stereonet projection. Note that S and Z are equivalent to “left-handed” and “right-handed” rotations, where the thumb is extended in the direction of the axis, and the remaining fingers curl in the direction of rotation. For an asymmetric fold, the internal rotation axis is equivalent to the fold axis, which can be measured in the field and plotted stereographically. For a Riedel composite structure, the internal rotation axis lies in the Y-surface and is parallel to the intersection of Y with either R or P. The intersection is calculated from the attitudes of Y, R, and P measured in the field. The sense of rotation, S or Z, assigned to the internal rotation axis is inferred from the geometry of the structure (fig. 8). Rutter and others (1986, fig. 11), who studied a fault gouge in Spain, used a similar procedure, but they did not report the sense of shear associated with individual Riedel structures.

In accord with the assumptions underlying our method, figure 10C shows the hypothesized distribution of S and Z internal rotation axes for a group of related structures produced in a fault zone. The axes all lie near a common plane, which parallels the attitude of the fault zone in which they formed. The monoclinic symmetry of the distribution is indicated by the single mirror plane, which lies perpendicular to the shear plane and bisects the two groups of S and Z axes. For this case, we infer that the *synoptic slip vector* for the fault zone lies at the intersection of the mirror plane and the plane of the fault zone. This vector can be viewed as the average direction of slip in the fault zone. In defining the slip vector, we use a footwall-fixed convention, that is, the slip vector corresponds to the direction of motion of the hangingwall relative to a fixed footwall. The *synoptic internal rotation axis* lies in the shear plane and is normal to the mirror plane. Note that the schematic example given in figure 10C shows the internal rotation axes dispersed around the synoptic internal rotation axis; this distribution is meant to illustrate the variations produced by stochastic processes.

Analysis of synoptic diagrams.—In our study, we have developed a specific procedure for identifying the main symmetry elements in synoptic diagrams. This procedure is illustrated here (fig. 11) using a computer-generated set of internal rotation axes for a moderately southwest-

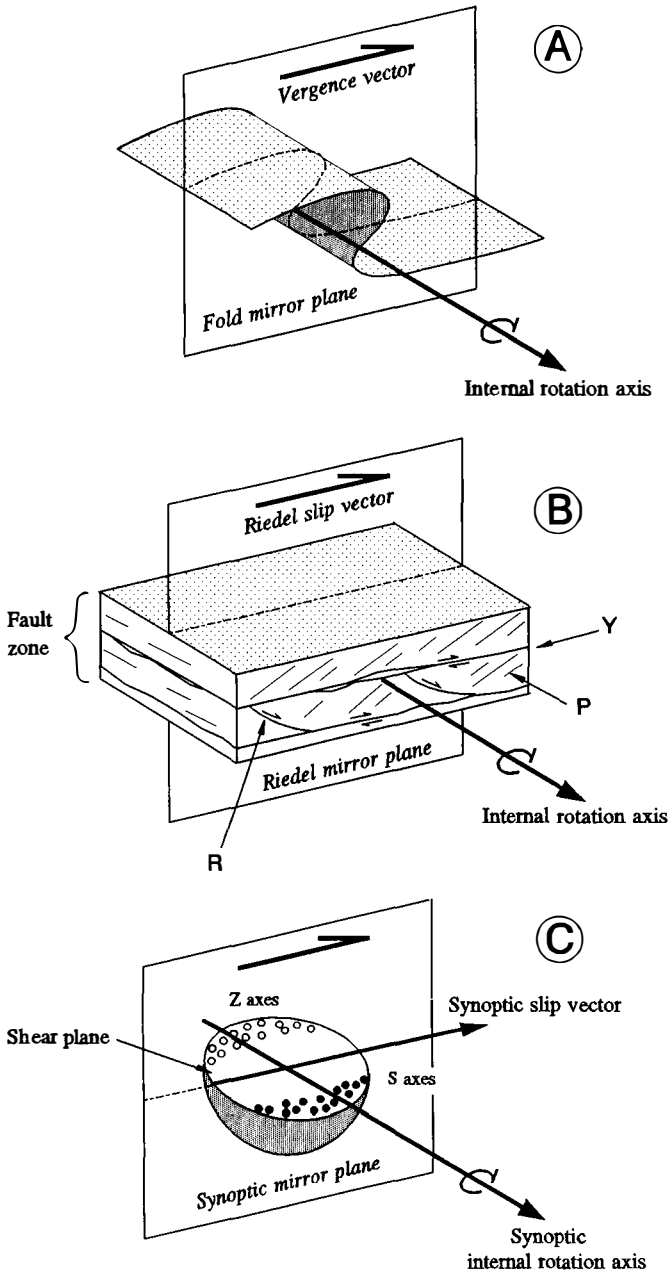


Fig. 10. Internal rotation axes represent the orientation and asymmetry of (A) meso-scale folds and (B) Riedel composite structures. The stereogram in (C) illustrates a dispersion of individual internal rotation axes about a mean direction, labelled as the synoptic internal rotation axis. The geometric relationship of this axis to an idealized shear zone with monoclinic symmetry is discussed in the text.

dipping thrust fault (attitude = 135° , 40°S) with a slip vector of 352° , -27° , corresponding to a top-to-the-north sense of slip. The distribution of axes (fig. 11A) was generated by random selection from a bivariate Gaussian distribution with a mean direction corresponding to the two synoptic internal rotation axes. The synoptic rotation axis is a symmetry element of the deformation (fig. 10C); in data from actual fault zones, it must be inferred from the distribution of measured axes. Random selection in this example resulted in overlapping clusters of S- and Z-axes. The synoptic S and Z axes lie in the shear plane (labelled G in fig. 11A) at 90° clockwise and anticlockwise, respectively, from the slip vector (labelled SV). The distribution mimics a girdle pattern because the angular deviation around the mean direction is much greater in a direction parallel to the girdle than in a direction perpendicular to the girdle. The first step is to find the average girdle for the distribution ($G = 137^\circ$, 39°S) and the associated pole to that girdle using the eigenvector method of Davis (1986, p. 334-339). For a monoclinic shear zone, the mirror plane (figs. 9 and 10) is perpendicular to the girdle and therefore includes its pole. By definition, the mirror plane must also bisect the clusters of S and Z axes.

The method we employed to find the mirror plane is graphically illustrated in figure 11. Using the strike and dip of the girdle as the rotation axis and rotation angle, respectively, the axes are rotated so that the girdle pattern coincides with the stereogram horizontal (Woodcock, 1979; fig. 11B). The resulting diagram is called a fault-parallel stereogram. Generally, this diagram better illustrates the symmetry of an orientation distribution relative to the fault plane. The strike and down-dip direction (labelled DDD) of the fault surface are shown for reference. In this diagram, we define the *azimuth* of an axis as its clockwise angle in the fault plane, as viewed looking down on the fault plane. Azimuth is measured relative to the strike. The azimuth of the strike line in a fault-parallel stereogram (fig. 11B) is set equal to the strike angle in the geographic stereogram (fig. 11A).

The rotation of the girdle to the stereogram horizontal carries some of the internal rotation axes into the upper hemisphere. The usual convention is to invert these axes through the origin and into the lower hemisphere and to invert their sense of rotation (S or Z) as well. This exercise shows that the designation of S or Z is not an intrinsic feature of an internal rotation axis but instead is a result of the direction in which we choose to view the structure. Therefore, in preparing our fault-parallel stereograms, we have chosen to convert all internal rotation axes to a common Z-sense of asymmetry. We refer to the new set of axes as Z-transformed axes. Our choice of a Z-transformation is completely arbitrary; we could just as well construct a set of S-transformed axes. However, when the data are Z-transformed, all the vectors will have a "right-handed" sense of rotation, which is the convention used by Means and others (1980) for vector calculations involving internal rotation axes. The Z-transformed axes will include both upper and lower hemisphere directions; these are shown without distinction. In other words, there is

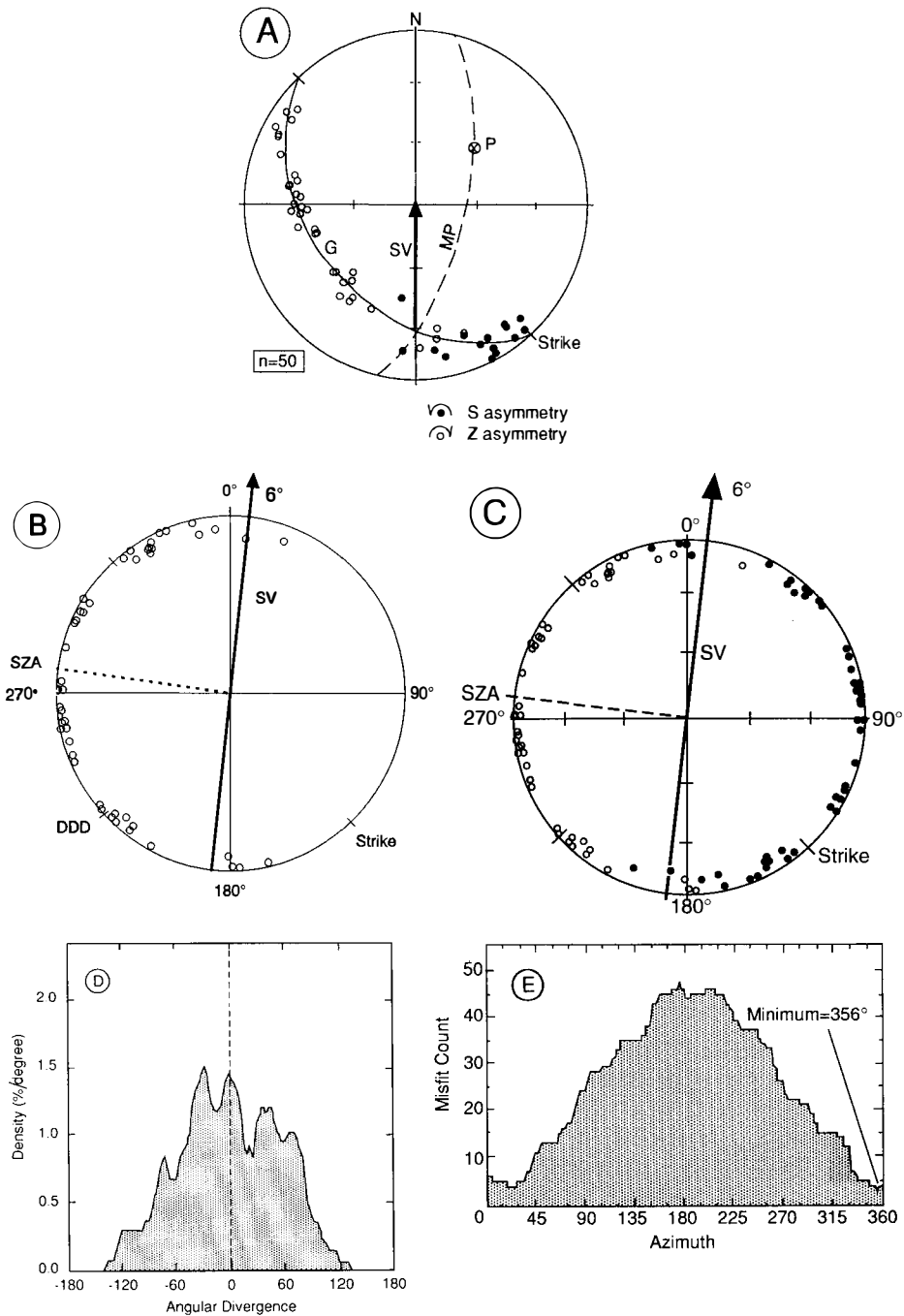


Figure 11

no way to determine in a fault-parallel diagram whether a transformed axis lies above or below the stereogram horizontal. At this point, it might appear that the diagram (fig. 11B) no longer has a plane of mirror symmetry. Each Z axis, however, is related to a completely equivalent S axis lying in the opposite direction. Both sets of axes are shown in figure 11C. It is these two distributions that give rise to a mirror symmetry plane. In our fault-parallel stereograms, only the Z-transformed axes are shown; the complementary S-transformed axes are implicit.

We have considered two different methods for defining the best-fit mirror plane. The *mean method* (compare Woodcock, 1979) is based on the expectation that the direction of the synoptic Z-axis corresponds to the average orientation of the Z internal rotation axes. (In some unusual cases the synoptic Z axis will lie at 90° to the average direction for the Z axes. See the Discussion for an example.) We propose that internal rotation axes are subjected to variations from this average direction because of stochastic and antecedent processes, which will produce a symmetric Gaussian distribution around the synoptic Z-axis, if, in fact, all these processes are random.

On this basis, the best-fit direction of the synoptic Z-axis, as determined by the mean method, corresponds to a direction in the girdle

Fig. 11. An illustration of the methods used to interpret synoptic diagrams of internal rotation axes. The dataset was generated by computer and was constructed assuming an idealized southwest-dipping thrust fault (attitude = $135^\circ, 40^\circ\text{S}$) with a synoptic slip vector of $352^\circ, -27^\circ$, indicating top-to-the-north sense of slip. Note that in these stereograms and others, the reported number of axes may appear to conflict with the number of axes plotted because of overlapping symbols. Also note that all stereograms are equal-area projections. (A) Lower hemisphere stereogram in present geographic orientation showing a girdle distribution of axes lying subparallel to the attitude of the fault zone. The axes are used to calculate an average girdle ($G = 137^\circ, 39^\circ\text{S}$) and associated pole (P). Lying normal to and within this girdle are the mirror plane (MP) and slip vector (SV), respectively, both of which are determined below. (B) Fault-parallel stereogram of Z-transformed axes. All axes are converted to a common sense of rotation (Z) and then rotated using the strike and dip of G as an axis and a rotation angle so that the fault zone lies parallel to the stereogram horizontal (primitive circle). The strike and down-dip direction (DDD) of the original fault surface are shown for reference. The diagram includes both upper and lower hemisphere axes plotted without distinction. For the mean method, the azimuth of the synoptic Z-axis (SZA) is estimated by the circular mean of the azimuths of the Z-transformed axes. By definition, the slip vector lies in the girdle plane and is orthogonal to synoptic Z axis and parallel to mirror plane. The geographic orientation of the slip vector is calculated by rotating the fault plane back to its initial orientation. (C) Fault-parallel stereogram illustrating the mirror-plane symmetry of the distribution shown in (B). Typically, the fault-parallel diagrams show only Z axes. In this diagram, each axis is represented by both its Z and S complements. For the mean method, the mirror plane is considered to be orthogonal to the mean of both distributions. Therefore, in a statistical sense, the mirror plane symmetrically bisects the Z and S distributions. (D) Probability density distribution plot, showing the density of axes as a function of angular divergence from the best-fit synoptic Z axis with negative and positive corresponding to anticlockwise and clockwise angles, respectively. Density is determined using a counter window fashioned after the method of Kamb (1959), and is reported in units of percentage of the total distribution per degree. (E) Misfit plot, showing the number of contrary internal rotation axes as a function of slip-vector azimuth in the plane of the fault. For an Z-transformed set of axes, a contrary axis is defined as an axis with an angular divergence from the synoptic Z axis direction outside the range $\pm 90^\circ$. The misfit method considers the best estimate of the slip vector to be the azimuth with the smallest misfit count. The example shown here has a minimum misfit count of three at an azimuth of 356° . The angular range for the minimum in the misfit plot is similar to the separation angle in the Hansen method.

(shear plane) with an azimuth defined by the circular mean of the azimuths of the Z-transformed axes. In most cases, we have determined the circular mean assuming a circular Gaussian distribution of unidirectional vectors distributed over the range from 0° to 360° (Mardia, 1972; Davis, 1986, p. 314-321). An alternative is to use the largest eigenvector for the orientation distribution, which defines the average direction of the axes in three dimensions. The mirror plane can now be determined because the direction of the synoptic Z-axis is normal to the mirror plane, assuming that the synoptic distribution has a monoclinic symmetry.

The symmetry of the fault-parallel distribution of axes is more clearly displayed using a probability density distribution plot (fig. 11D; compare Woodcock, 1979; Platt, Leggett, and Alam, 1988). This plot shows the density of axes (percentage of the total distribution per degree) as a function of angular divergence, which is defined as the angle that an axis makes with respect to the best-fit direction of the synoptic Z-axis in the fault plane. Negative and positive values indicate anticlockwise and clockwise angles, respectively, assuming that we are looking down on the fault surface. The distribution displays a Gaussian-like form, which is expected given that the dataset was generated using a Gaussian model. In figure 11D, monoclinic symmetry is indicated by the symmetrical form of the probability density plot around the synoptic Z-axis, which marks the position of a two-fold rotation axis. Note that for distributions of axial vectors, the two symmetry operations—a reflection across a mirror plane and a two-fold rotation around the axis normal to the mirror plane—produce equivalent results. Because internal rotation axes are axial vectors, the rotation represented by the axis remains unaffected by inversion of its representative vector through the origin.

The alternative to the mean method is the *misfit method*, which is based on the premise that all the Z-transformed internal rotation axes should lie within an angular range of $\pm 90^\circ$ of the direction of the synoptic Z-axis. If an axis lies outside that range, its sense of rotation would be contrary to that predicted by the synoptic internal rotation axis. Therefore, the misfit method considers the best-fit slip vector to have an orientation where the number of misfit axes is at a minimum. This method is graphically illustrated by the misfit plot (fig. 11E), which shows the number of misfit axes as a function of the azimuthal position of the slip vector. For the computer-generated example, the minimum is located at an azimuth of 356° with a misfit count of three. This situation reflects the fact that the clusters of S and Z axes overlapped in the original geographic stereogram (fig. 11A).

In our experience, the mean and misfit methods produce similar results. Nonetheless, we prefer the mean method, because it utilizes the full dataset and better represents the overall symmetry of the distribution, whereas the misfit method is heavily influenced by a small fraction of the data located in the tails of the distribution. Table 1 shows the results of the mean method for the computer-generated example. The

TABLE 1
Summary of results as determined by the mean method

Type of Structure	Na/Nt*	Average shear surface (strike, dip)	Slip Vector**		Distribution Statistics		Misfit Count
			Geographic orientation (trend, plunge)	Azimuth in fault surface ($\pm 2SE$)	$\pm 2\sigma$ (circular std. deviation)	K-S Probability	
Computer-generated example	50/50	137°, 39°S	359°, -28°	6° \pm 16°	\pm 108°	76%	5
Hansen's Landslide	36/36	48°, 24°N	315°, 24°	45° \pm 15°	\pm 92°	100%	1
Lopez Structural Complex							
Asymmetric folds	33/55	116°, 64°N	176°, -61°	192° \pm 9°	\pm 52°	64%	0
Rosario fault zone							
Asymmetric folds	77/82	121°, 36°N	250°, -30°	244° \pm 18°	\pm 139°	90%	17
Riedel structures†	57/57	127°, 36°N	313°, 7°	226° \pm 7°	\pm 56°	94%	NA

* Number of asymmetric structures versus total number of structures measured.

** Slip direction of hangingwall relative to a fixed footwall. Positive (negative) plunge indicates downward (upward) directed motion. The uncertainty for the azimuth is ± 2 standard error. The "geographic orientation" is the slip vector in the present geographic reference frame. The "azimuth" is the orientation of the slip vector in the fault-parallel stereogram.

† Mean direction and distribution statistics calculated using a bidirectional (bimodal) model (see text).

best-fit slip vector agrees well with the values used to construct the dataset. The geographic orientation of the slip vector is determined by applying the inverse of the rotation used to construct the fault-parallel stereogram. The uncertainty for the slip-vector azimuth is based on the estimated two standard-error uncertainty for the best-fit azimuth of the synoptic Z-axis.

The overall distribution is represented by two statistical parameters (table 1). The circular standard deviation provides a measure of the degree of dispersion of the axes around the calculated direction of the synoptic Z-axis. The range is given as \pm two standard deviations, which should include about 95 percent of the distribution. The K-S probability refers to the Kolmogorov-Smirnov test (Press and others, 1986) which gives the probability that departures from a circular Gaussian distribution are due to random chance alone. A high probability indicates that the azimuth distribution for the axes is not significantly different from that predicted for a symmetric Gaussian distribution. The computer-generated example has a probability of 76 percent, indicating a good match.

The misfit count (table 1) indicates the number of Z-transformed axes that lie outside the angular range $\pm 90^\circ$ with respect to the direction of the synoptic Z-axis. In the misfit method, these axes would be considered to have a rotation sense contrary to that predicted by the synoptic Z-axis.

Hansen's landslide.—As a test of our method, we applied it to the asymmetric folds in Hansen's (1967, 1971) tundra landslide (fig. 12). The results, recorded in table 1, show that the fold axes have a well-defined Gaussian distribution symmetric about the synoptic Z-axis. The synoptic slip vector determined by our method is virtually identical to the observed slip direction of the landslide.

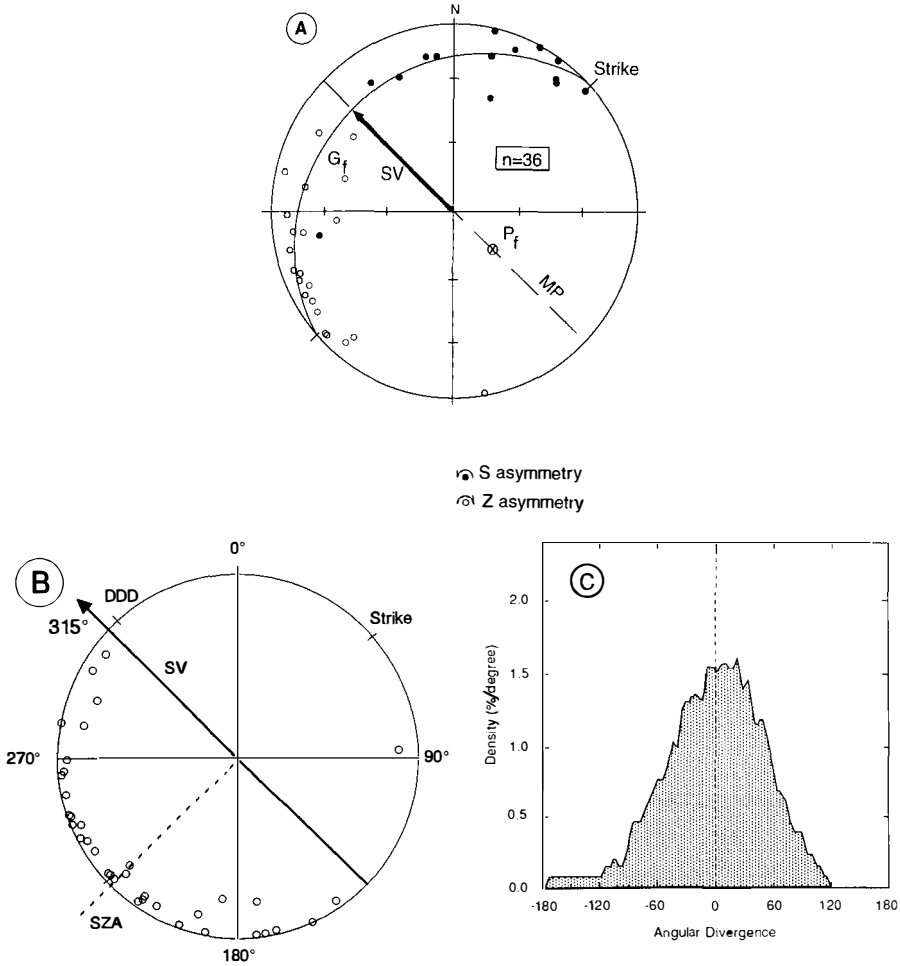


Fig. 12. An analysis of asymmetric folds from the tundra landslide described by Hansen (1967, 1971). We applied the same method used for the computer-generated example (figs. 11 and 12; note that the same symbols are used throughout). (A) lower hemisphere stereogram of fold axes in present geographic orientation. The great circle represents the "fault" plane, which dips northwest. The landslide (hangingwall) slipped northwest, relative to a fixed footwall. (B) Fault-parallel stereogram of Z-transformed axes. (C) Probability density distribution plot.

FAULT-RELATED STRUCTURES IN THE LOPEZ STRUCTURAL COMPLEX

The Lopez Structural Complex, like the Rosario zone, includes numerous cataclastic shear zones, but Riedel structures are rare. Instead, the dominant fabric element in both fault lenses and associated shear zones is a solution-mass-transfer cleavage, which clearly postdates fault-related fragmentation and imbrication, as described above. When we mapped the Lopez Complex in its entirety for an earlier study (Brandon, Cowan, and Vance, 1988), we noted that mesoscale folds might provide kinematic information about the fault zone.

Mesoscale Folds

The Lopez Complex features two types of folds. The majority are flexural-slip folds in meter- to kilometer-thick fault-bounded lenses of either interbedded turbidite sandstone and mudstone or radiolarian ribbon chert (fig. 13A). Amplitudes range from about 0.2 to 2 m. Some of these folds might have formed prior to faulting. We think that this possibility is limited to only a small fraction of the folds because folds are rare in the units that bound the Lopez fault zone (Constitution Formation; Brandon, 1980; Decatur terrane; Garver, 1988).

Less common in the Lopez Complex are centimeter-scale, open to isoclinal flexural folds defined by isolated fragments of chert or sandstone layers surrounded by mudstone-rich cataclasite. We are confident that folds of this type originated as a result of faulting, because they developed in fragments that were themselves plucked or sliced off larger lenses and incorporated into mesoscopically ductile, cataclastically flowing matrix. Field relations (fig. 13A) do show that all Lopez folds predate the solution-mass-transfer cleavage.

About half the folds are asymmetric and locally slightly overturned; the remainder are either ambiguous or, in rare cases, symmetric. All the asymmetric folds verge consistently to the southwest or south. On a stereogram (fig. 14A), the best-fit girdle for the fold axes is subparallel to the overall attitude of the Lopez Complex and the faults inside the complex. Fold axes are clearly separated into two groups of opposing asymmetry with a separation angle of 54° . The constructed slip vector (fig. 14B) indicates top-to-the-south transport. The misfit count is zero. The probability density distribution plot (fig. 14C) shows a relatively tight cluster of axes around the direction of the synoptic Z-axis; the cluster covers a range of about $\pm 52^\circ$ (equivalent to $\pm 2\sigma$). The K-S probability (64 percent) indicates that the Gaussian model fits the distribution well.

It is instructive to consider the fold data as represented by vergence vectors in map view (fig. 15). A vergence vector for a fold is constructed to lie in the plane of shear and perpendicular to the fold axis (fig. 10A). Although each vergence vector has a direction compatible with the shear sense of the fold, the arrow is not necessarily parallel to the local slip vector responsible for the fold. The map shows a wide dispersion of vergence vectors, from which it is nearly impossible to deduce the synoptic slip vector by inspection alone.

A.



Fig. 13. Photos of mesoscale fault-related structures. (A) Asymmetric horizontal folds in radiolarian ribbon chert in Lopez Complex. View is parallel to fold hinges, looking toward the northwest. S-asymmetry and anticlockwise rotation define a local top-to-the-southwest vergence. The solution-mass-transfer cleavage superimposed on fault rocks and lenses in the Lopez zone appears as a spaced foliation roughly parallel to the axial planes of the folds.

B.

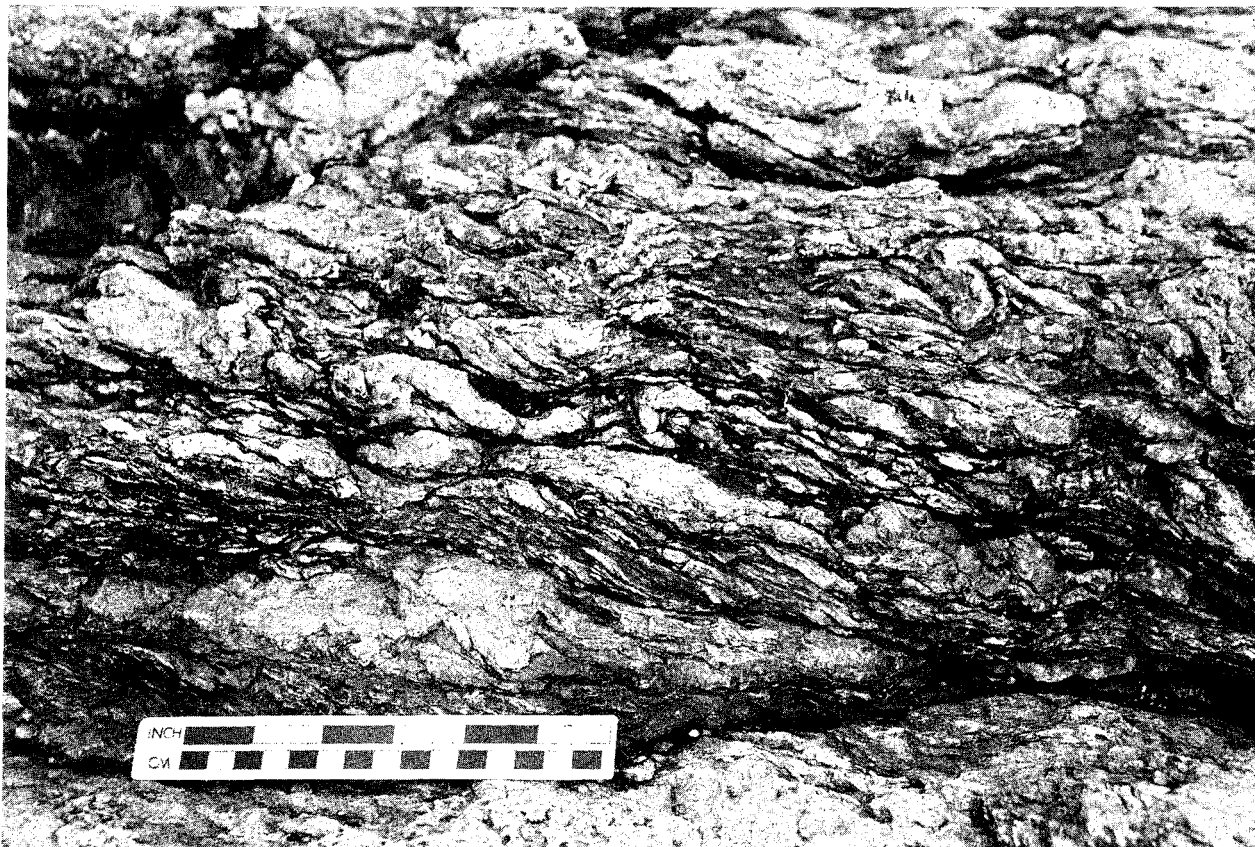


Fig. 13(B) Generally chaotic aspect of fault rock, derived largely from Orcas Chert, in the Rosario fault zone, San Juan Island. Light fragments and lenses are chiefly remnants of chert layers dispersed in dark mudstone. Note the asymmetric fold in the upper right quadrant (S-asymmetry; anticlockwise internal rotation axis; local vergence direction top-to-left).

C.

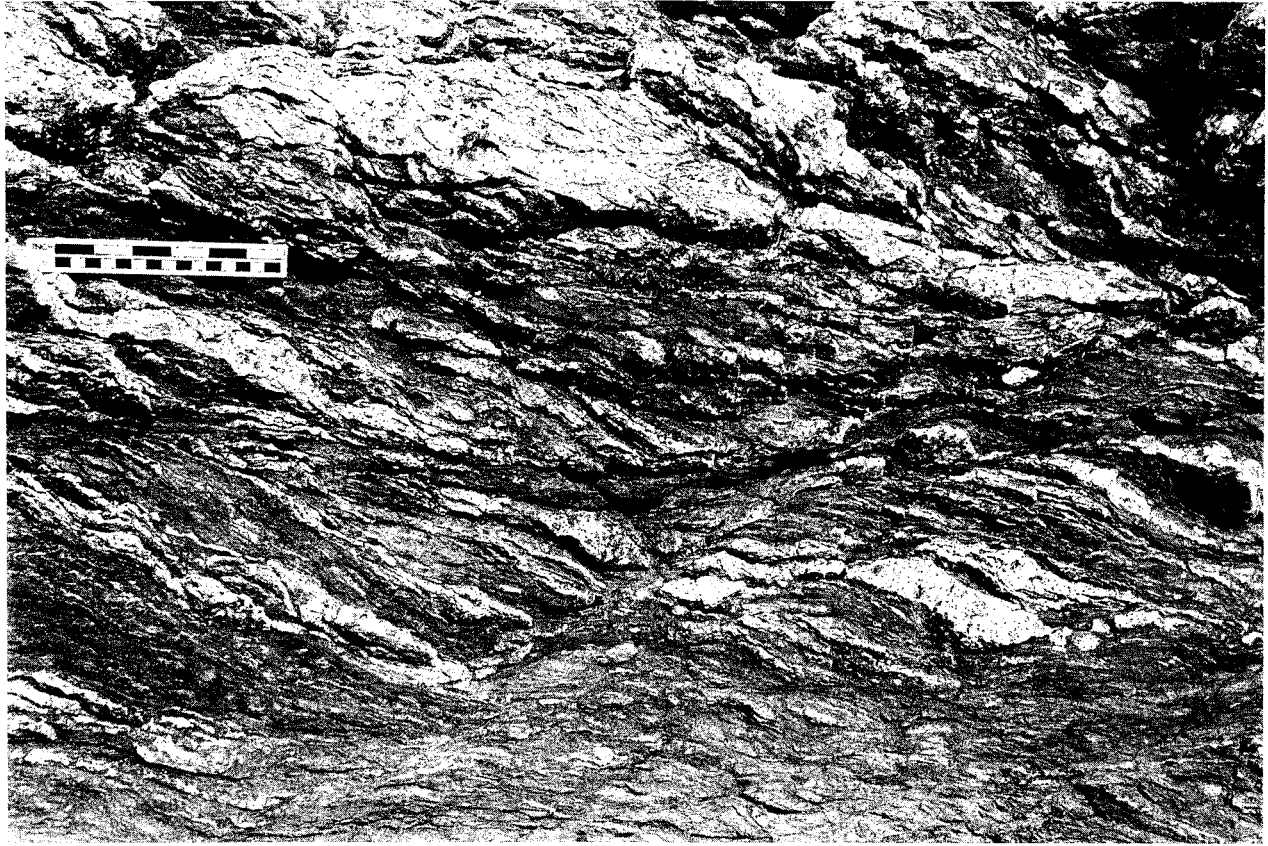


Fig. 13(C) Riedel composite structure in Rosario fault zone. Most of the outcrop consists of foliated cataclasite; light fragments and lenses are chiefly chert, and darker "matrix" includes mudstone and cataclastic mafic volcanic rocks. Ruler is parallel to and lies on a Y-structure. P is the penetrative cataclastic foliation dipping toward the right. A prominent R-structure crosses the lower center and dips left. In this view, normal slip along R is indicated by deflection of the P foliation. As viewed in this photograph, the internal rotation axis for this Riedel structure is anticlockwise; local slip vector is top-to-the-left (sinistral) (compare with fig. 8).

D.



Fig. 13 (D) Riedel structure in Orcas Chert within the Rosario fault zone. Hammer head is parallel to Y and lies on a Y-surface. R structures dip left and show normal (down-to-the-left) offset of chert layers. Orientation of chert layers is geometrically appropriate for P. Local slip vector is top-side-to-the-left (compare with fig. 8). This outcrop was photographed by Maekawa and Brown (1991, fig. 11), who described the features as due to "fault drag."

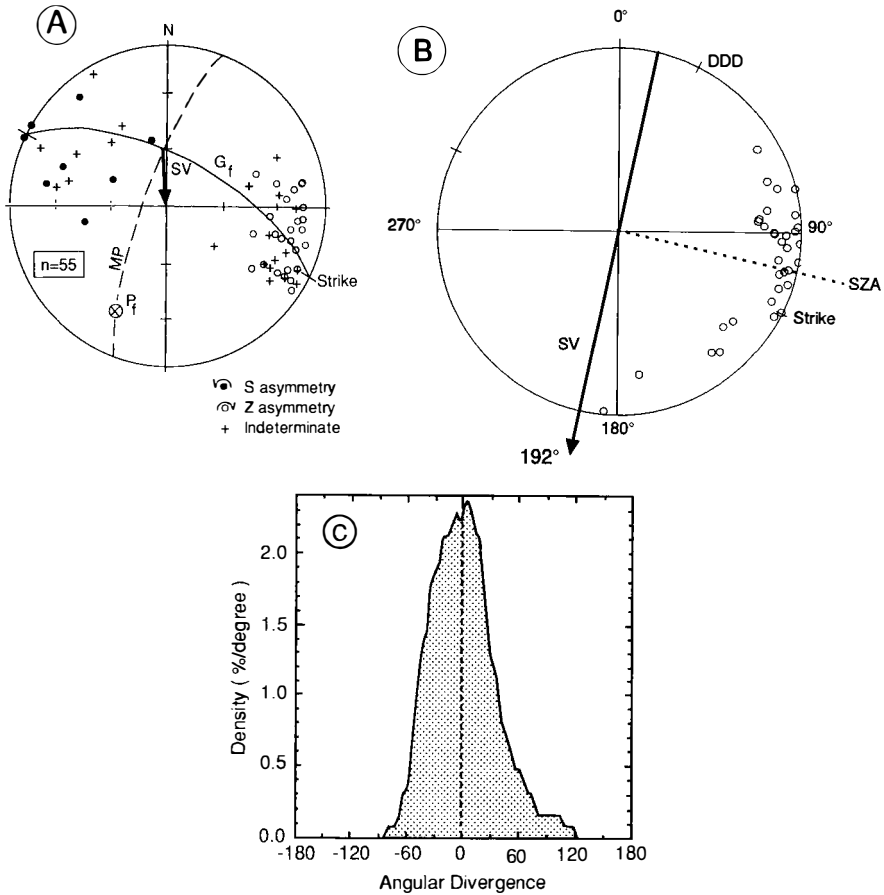


Fig. 14. Synoptic analysis of mesoscale folds in the Lopez fault zone. (A) Lower hemisphere stereogram of internal rotation axes in present geographic orientation. G_f = average girdle for the fold axes. P_f = pole to G_f . MP and SV are the inferred mirror plane and slip vector, respectively. (B) Fault-parallel stereogram of Z-transformed axes. G_f was used to determine the axis of rotation. SZA is the best-fit synoptic Z axis. (C) Probability density distribution plot, showing a symmetric distribution clustered within about $\pm 60^\circ$ of the synoptic Z axis direction.

FAULT-RELATED STRUCTURES IN THE ROSARIO ZONE

We examined all accessible parts of the Rosario fault zone along a 12 km segment of the southwest coast of San Juan Island from Deadman Bay to South Beach (fig. 4). Overall, the fault zone has a well-organized macroscopic internal structure defined by fault slices within the zone and also by bedding within some fault slices; all these surfaces strike northwest and dip moderately to the northeast. At outcrop scale, however, most of the rocks appear to have been deformed in a disorganized or

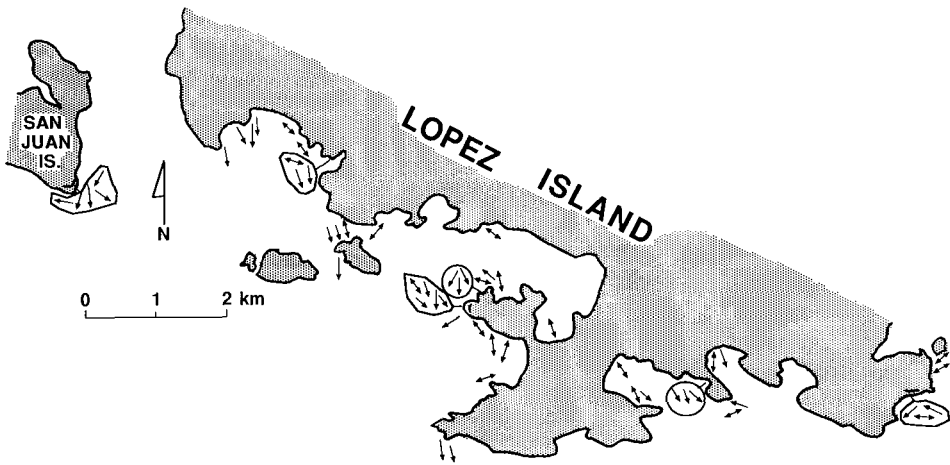


Fig. 15. Map showing the trend of vergence vectors for mesoscale folds in the Lopez Complex. The same folds are plotted stereographically in figure 14A and B. A vergence vector, as used here, is perpendicular to the fold hinge, parallel to the shear plane (that is, G_1 in fig. 14), and points in the direction consistent with the sense of shear implied by the fold, assuming a footwall-fixed convention (see fig. 10A). This figure illustrates the large angular dispersion among the individual kinematic indicators. Single-headed arrows represent asymmetric folds; double-headed, symmetric or ambiguous folds. All arrows are plotted offshore, adjacent to where folds crop out along the coast. Where several measurements were made at one outcrop, the arrows are shown in a circled group.

chaotic manner (fig. 13B, C). For example, chert beds are locally discontinuous or contorted, and lenses of chert, sandstone, or basalt typically are separated by irregular zones of indurated, foliated to massive cataclastite. The Rosario fault contains both asymmetric folds and Riedel structures and is locally overprinted by the solution-mass-transfer cleavage.

Mesosopic Cataclastic Flow

There is abundant evidence that cataclastic flow was an important mode of deformation in the Rosario fault zone. On a mesoscopic scale, lenses of chert, sandstone, and basalt are bounded either by anastomosing faults or by lenses and irregular zones of fine-grained, indurated cataclastite. Thin-section observations show that the cataclastites were formed by fracturing, crushing, and abrasion of mineral grains, which resulted in an overall reduction in grain size. We have observed little evidence of recrystallization associated with cataclastic deformation except in ribbon chert, which now contains patches and veins of microcrystalline quartz. Diffusion, recrystallization, and healing of fractures might have been promoted in this rock type by fluids in the fault zone. The prevalence of frictional, as opposed to temperature-activated, deformation mechanisms accords with the independent evidence provided by very low-grade metamorphic assemblages and fission-track ages, which

indicate that temperatures in the Rosario fault zone did not exceed about 175°C (Brandon, Cowan, and Vance, 1988).

In outcrops and hand specimens, the color of the cataclasite reflects its protolith. Olive-green cataclasites were derived from pillow basalts, or mafic schists of the Garrison Schist, and black cataclasites from mudstone. In contrast, chert and sandstone commonly form angular and lenticular fragments (fig. 13). These cataclasites commonly preserve evidence of mesoscale ductile behavior. For example, green and black components are irregularly mixed and swirled together, or the fine-grained matrix, charged with inclusions, has invaded fractures and re-entrants in centimeter- to meter-scale fault lenses. In most cases, outcrops dominated by cataclasites have a chaotic aspect, but locally they display well-defined penetrative or semi-penetrative planar structures which maintain a consistent geometry on the scale of a few meters (fig. 13C).

Mesoscale Folds

Mesoscale folds, with amplitudes ranging from about 1 to 50 cm, are defined chiefly by fragments of chert beds in fault-generated cataclasite and also by bedded ribbon chert, layers of chert in basalt, and foliated cataclasite. As in the Lopez Complex, folds are restricted to the Rosario fault zone and are uncommon in units that bound the fault zone. Most folds are detached, involving only an isolated single layer. Because the majority of the analyzed folds are either immersed in cataclasite or situated adjacent to fault surfaces, we interpret their final orientation and geometry as related to fault-zone deformation. There is no evidence to indicate that these folds originated as larger, more coherent trains. For our study, we measured only well-formed folds that were clearly asymmetric when viewed in profile. They constituted about 10 percent of all folds in the fault zone. For the remaining 90 percent, the sense of asymmetry was indeterminate.

The axes of asymmetric folds are plotted in figure 16. Local vergence vectors are depicted in map view in figure 17. In the stereogram (fig. 16A): (1) the internal rotation axes define a plane with an attitude subparallel to the Rosario fault zone, and (2) the axes cluster into two groups of opposing asymmetry, but because of extensive overlap, there is no separation angle between the two groups. The slip vector estimated using the mean method has an azimuth in the fault-parallel stereogram (fig. 16B) of 244° and a geographic orientation of 250°, -30°, indicating top-to-the-southwest transport. The misfit count (table 1) is fairly large; 17 axes out of a total of 77 have a sense of rotation contrary to that implied by the best-fit direction of the synoptic Z-axis. The distribution of axes around the direction of the synoptic Z-axis (fig. 16C) is symmetric and fits the Gaussian model well (K-S probability is 90 percent). Nevertheless, the axes are dispersed over a large angular range, about $\pm 139^\circ$. This dispersion is also apparent in figure 17 which shows the trend of vergence vectors for the asymmetric folds. The wide overlap of S- and Z-folds evident in figure 16A and the consequent wide dispersion of

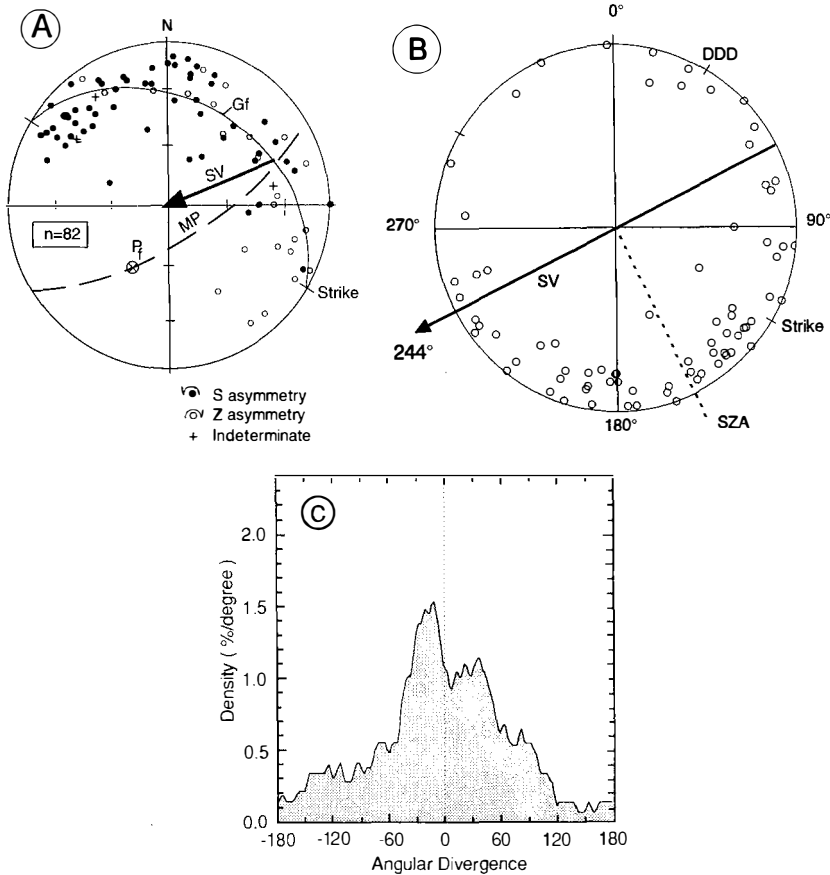


Fig. 16. Synoptic analysis of mesoscale folds in the Rosario fault zone. (A) Lower hemisphere stereogram of internal rotation axes in present geographic orientation. G_f = average girdle for the fold axes. P_f = pole to G_f . MP and SV are the inferred mirror plane and slip vector, respectively. (B) Fault-parallel stereogram showing Z-transformed axes. G_f was used to determine the rotation. SZA is the best-fit synoptic Z axis. (C) Probability density distribution plot, showing a broad dispersion of axes around the synoptic Z axis direction.

internal rotation axes in figure 16b contrast with the distinctly separated groups of asymmetric folds in Hansen's landslide (fig. 12) and the Lopez fault zone (fig. 14). We consider the origin of this pattern in the Discussion below.

Riedel Structures in Cataclasites

To justify using composite planar structures in our kinematic analysis, we need to establish that: (1) they are analogous to experimentally produced structures, which have an unambiguous geometrical relationship to the boundaries and slip vector of a shear zone; (2) the components

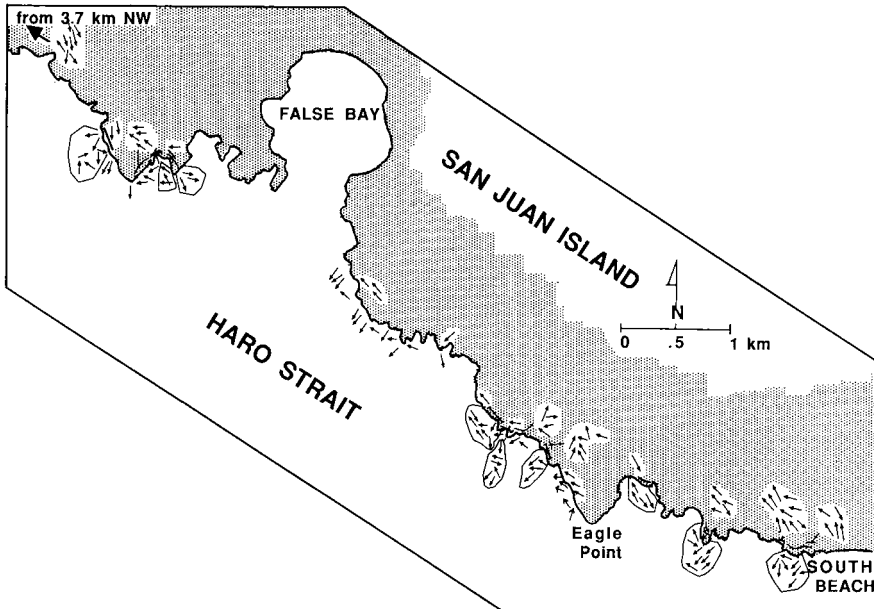


Fig. 17. Map depicting the trend of local vergence vectors for folds (arrows plotted offshore) and slip vectors for Riedel structures (arrows plotted on land) in the Rosario fault zone.

of an individual Riedel structure can be reliably identified as Y, R, or P; and (3) each structure is related to fault-induced deformation in the Rosario zone. Concerning the first two points, our use of Riedel structures closely parallels the approach of Rutter and others (1986) and Chester and Logan (1987). We restricted our field measurements to individual shear zones that range from 0.1 to 1 m in thickness and that meet the following criteria: (1) They are bounded by continuous, roughly planar, subparallel faults, which we interpret as Y-surfaces or primary displacement surfaces. Some shear zones contain one or more additional Y-surfaces. (2) They include secondary planar structures oblique to Y and designated as R and P, as defined below.

In our study, the following criteria were used to identify Y-, R-, and P-structures. Y-surfaces truncate layering and foliation and locally juxtapose different rock types (for example, chert and basalt, or cataclasite). At the mesoscopic scale, it is not possible to match offset markers across Y nor to determine the sense of slip. In contrast, the R-structures, when viewed in sections approximately normal to both Y and R, look like small normal faults (compare figs. 8 and 13C). The acute angle between Y and R ranges from about 15° to 45° , with an average of 31° . In every case, the sense of slip, and, in most cases, the amount of slip (averaging a few centimeters) can be determined using offset markers (bedding or cataclas-

tic foliation) and the deflection of the layering as it approaches the R-surface. The R-surfaces are equivalent to the familiar "Riedel shears" *sensu strictu* (R_1) of Logan and others (1979). As a result of their orientation and displacement, R-shear surfaces contribute to local thinning of the shear zone and also add to the amount of slip on Y. In this sense, R-structures can be referred to as additive shears (Suppe, 1985). We use the orientation of R to determine the local sense-of-shear on Y. The acute angle between R and an overlying Y opens in the direction of the slip vector, assuming a footwall-fixed reference frame.

Natural and experimental brittle shear zones also display two kinds of planar structures having an inclination, with respect to Y, opposite that of R (fig. 8). For example, Logan and others (1979) describe P-fractures, which are shear fractures that have accommodated reverse, rather than normal, slip in sections perpendicular to the overall slip vector. Other workers, notably Tchalenko (1968), Rutter and others (1986), and Chester and Logan (1987), have described a penetrative cataclastic foliation, defined by the parallel preferred orientation of phyllosilicates, tabular fragments, or compositional layering, that is inclined to Y in the same sense as the P-fractures. We follow Rutter and others (1986) and use the term "P-foliation" for this penetrative mesoscale cataclastic foliation.

In the Rosario fault zone, P-foliation predominates; P-fractures were not observed. The penetrative character of the foliation allows it to be identified uniquely as P rather than R, even where R-shear fractures are absent. The P-foliation can also be differentiated from the solution-mass-transfer cleavage, because the P foliation is restricted to discrete brittle shear zones and is defined mainly by the preferred orientation of the shapes of cataclastic fragments (fig. 13C). We use the intersection of the P-foliation with Y to define a fabric element. Our kinematic inference—that this intersection is an internal rotation axis—is based on experimental and field evidence. We acknowledge, however, that the processes and mechanisms that form the P-foliation are not fully resolved.

Regarding the third point raised above, it is certain that each Riedel structure measured and analyzed in this study developed in local, centimeter- to meter-scale, non-coaxial shear zones. These zones are distributed throughout the Rosario fault zone and so record part of the bulk deformation of the fault rocks within the Rosario zone. Neither the overall symmetry of macroscopic shear nor the orientation of a bulk slip vector is evident from inspection of the field evidence alone. Rather, this evidence indicates that slip vectors determined from individual Riedel composite structures are widely dispersed in the plane of the fault zone (fig. 17). Moreover, at South Beach, a single outcrop contains Riedel structures with opposing asymmetry, and yet these structures are separated by only a few meters. Nonetheless, the critical question is, does the orientation distribution for the Riedel structures reveal the monoclinic symmetry of the deformation? We can test for the presence of a mirror plane by comparing the distribution of internal rotation axes with that predicted for a Gaussian distribution. A successful test would indicate

that the distribution is statistically symmetric around the synoptic Z-axis, as required for monoclinic symmetry.

The field procedure involved measuring the attitudes of related Y-, P-, and R-surfaces in individual shear zones. The intersections in each set were calculated and plotted by computer. The synoptic analysis is shown in figure 18. The internal rotation axes display a clear girdle pattern. The coincidence of this girdle with the average attitude of Y (P_y in fig. 18A) provides a test of the internal consistency of our data. The average orientation of Y-structures is also subparallel to the girdle defined by fold axes from the Rosario fault zone (fig. 16A), which in turn is roughly parallel to the map-scale attitude of the entire fault zone. In the fault-parallel stereogram (fig. 18B), the Z-transformed axes show considerable dispersion, covering virtually the entire azimuthal range in the fault plane. The probability density distribution plot (fig. 18C) shows two modes that are separated by about 180° . Using a unidirectional circular Gaussian model, we determined a mean azimuth of 216° and a K-S probability of 2 percent. Clearly, this model fails to represent the data. A bidirectional circular Gaussian distribution (Mardia, 1972) provides a more reasonable fit to the data (K-S probability = 94 percent). A bidirectional distribution is made up of two Gaussian distributions that have means separated by 180° and equal standard deviations. This symmetric bimodal distribution illustrates the fact that there are two populations of Riedel structures, distinguished by opposite shear sense: 75 percent of the structures (43 out of 57) formed with their Z axes clustered around an average azimuth of 226° , whereas 25 percent (14 out of 57) formed with their Z axes clustered around an average azimuth of 46° . Field observations preclude the explanation that the different populations are restricted to different macroscopic structural domains in the study area, because such domains are not apparent in the map of slip vectors (fig. 17).

In a strict sense, the symmetry of the distribution in figure 18 is monoclinic; the two modes are not fully symmetric because of their unequal size. If this were the case, the distributions of folds and Riedel structures for the Rosario fault zone would have no symmetry elements in common, except for a center of symmetry, and the total fabric would be triclinic. We suggest, however, that the difference in size of the modes may be due to a sampling problem. In other words, our study area was not large enough to capture a statistically homogeneous population of Riedel structures. On this basis, we propose that the symmetry of the distribution of Riedel structures is orthorhombic, and in figure 18A and B we identify the three orthogonal mirror planes that include the girdle of internal rotation axes and their mean direction. (Eigenvectors of this distribution could be used to determine these mirror planes.)

If the symmetry of the distribution is in fact orthorhombic, then the mirror plane for a postulated deformation with monoclinic symmetry (fig. 9) could correspond to either of the three mirror planes of the distribution. However, the distributions of folds and Riedel structures

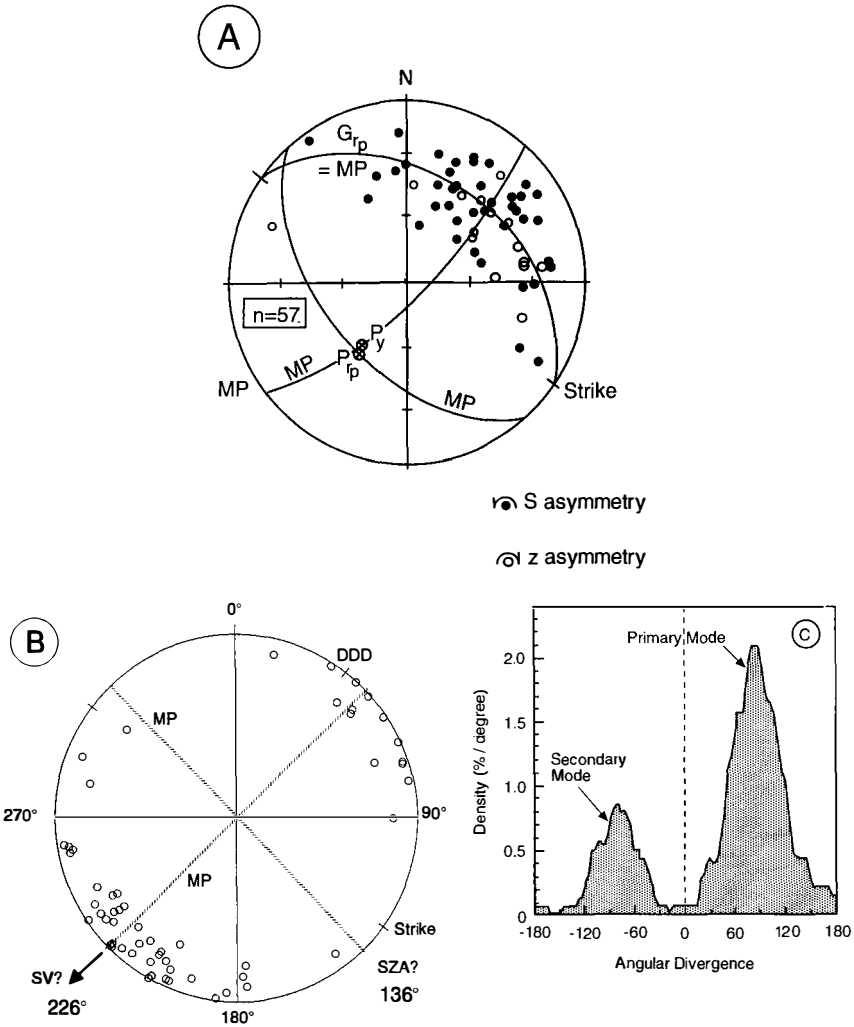


Fig. 18. Synoptic analysis of Riedel structures in the Rosario fault zone. (A) Lower hemisphere stereogram of internal rotation axes in present geographic orientation. G_{rp} = average gridle for the Riedel internal rotation axes. P_{ip} = pole to G_{rp} . P_y = average pole for Y surfaces. Note that the poles P_y and P_{ip} are nearly parallel as would be expected given the geometry of the Riedel structure. MP marks the three mirror planes inferred to be present in this subfabric. The slip vector is ambiguous and thus is not shown in this figure. (B) Fault-parallel stereogram showing Z-transformed axes. G_{rp} was used to determine the rotation. SZA and SV mark the inferred orientations for the inferred synoptic Z axis and the slip vector. (C) Probability density distribution plot, showing a bimodal distribution of axes with the synoptic Z axis bisecting the modes.

would share a common, steeply dipping mirror plane that strikes north-east-southwest (compare figs. 16A and 18A). On the basis of the monoclinic symmetry of the total fabric, we deduce the synoptic Z-axis and the slip vector for the fault-zone deformation to lie perpendicular and parallel, respectively, to this mirror plane, as shown in figure 18B. This interpretation leads to an unusual relationship: the synoptic Z-axis for the deformation is considered to lie at 90° to the average direction of the Z-axes for the Riedel structures. We address this relationship in the Discussion below.

DISCUSSION

Folds in the Lopez and Rosario Fault Zones.—The distributions of internal rotation axes (figs. 14 and 16) have monoclinic symmetry compatible with that expected in our idealized shear zone (fig. 9). We use this symmetry to deduce the slip vector for each fault zone. In the Lopez zone and Hansen's landslide (fig. 12), rotation axes are more tightly clustered than those in the Rosario zone, but in all three cases, the data show a symmetric Gaussian distribution about a mean direction. We interpret this dispersion to be due to antecedent and stochastic processes. In the case of the Rosario zone, these processes resulted in a wide dispersion of fold axes (fig. 16A). This "messy" distribution retains monoclinic symmetry, however, and can be analyzed by our method, even though the distribution lacks the separation angle that Hansen (1967, 1971) used in his method.

A possible alternative hypothesis is that our orientation distributions have resulted from passive rotation of fold axes toward the direction of maximum extension (X). This process is inferred to have been responsible for the preferred orientation of fold axes in ductile mylonitic shear zones where shear strains are large ($\gamma > 10$; for example, Bell, 1978; Malavieille, 1987). In this extreme case, the axes will be tightly clustered and might be expected to look similar to the pattern of clustered fold axes that we show above. However, after passive rotation by extreme extension, fold axes will be clustered adjacent to the mirror plane of the deformation and at a high angle to the synoptic Z axis (fig. 19B; see also fig. 10 in Sanderson, 1973; and fig. 2 in Woodcock, 1979). When the axes are transformed to Z and plotted on a fault-parallel stereogram, this distribution will show two modes separated by nearly 180° and bisected by the synoptic Z axis. In contrast, the distributions of our fold data are unimodal, so that the average direction of the distribution of Z axes lies parallel to the synoptic Z axis and not to the X direction (fig. 19A). Both types of fold-axis distributions (fig. 19A, B) have monoclinic symmetry.

Riedel structures in the Rosario fault zone.—We infer that the internal rotation axes of Riedel structures have orthorhombic symmetry (figs. 18 and 19C). For this interpretation to be valid, we must assume that the contrast in the size of the two modes is due to sampling errors. Each mode has a symmetric Gaussian distribution of internal rotation axes, which we ascribe to stochastic processes.

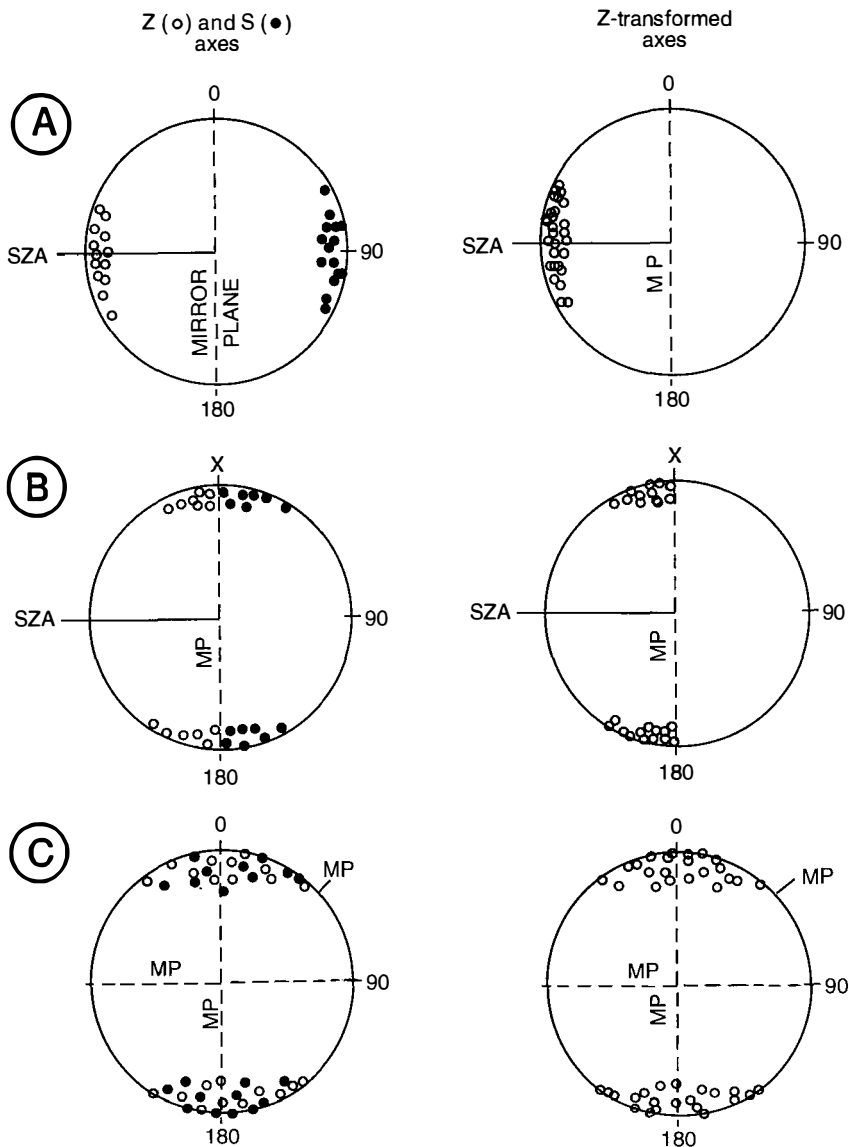


Fig. 19. Lower hemisphere stereograms illustrating symmetry elements for different types of distributions of internal rotation axes. (A) Ordinary symmetric dispersion around the synoptic Z-axis as predicted by the model of an idealized shear one (fig. 9). Monoclinic symmetry defined by a single mirror plane (MP). (B) Distribution expected to result from passive rotation after extreme extension parallel to the X direction of the bulk strain ellipsoid. Axes are clustered around the single mirror plane of monoclinic symmetry. (C) Distribution with orthorhombic symmetry defined by three orthogonal symmetry planes. The direction of the synoptic Z axis cannot be identified.

Orthorhombic symmetry is also evident in the orientation distribution of Y structures (fig. 20). Overall, Y is statistically subparallel to the Rosario fault zone and to the girdle representing fold axes within it (figs. 16A and 20). However, when distinguished by slip direction, the Y-structures separate into two groups differing in orientation by $\sim 15^\circ$. For the group that makes up the primary mode, slip was top-to-the-northwest (fig. 18B, C). For the other group, slip was in the opposite direction, top-to-the-southeast. The distribution of poles to Y (fig. 20) and the distribution of the internal rotation axes for the Riedel structures (fig. 18A) have the same three mirror planes.

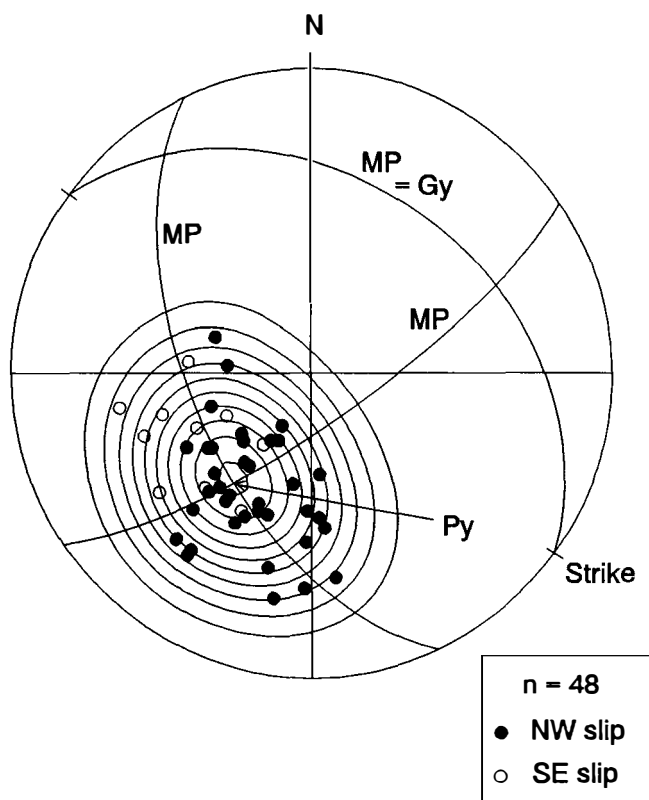


Fig. 20. Lower hemisphere stereograms showing poles to Y surfaces in the Rosario fault zone. The Y surface marks the primary slip surface in the Riedel structure. The average pole P, corresponds to the average attitude $G_1 = 126^\circ, 36^\circ\text{N}$ of the Y surfaces, which are subparallel to the overall fault zone. Two different groups of Y surfaces are apparent. One group (solid dot) has a general slip direction of top-to-the-northwest, and the other (open dot), top-to-the-southeast. The distribution has orthorhombic symmetry with three mirror planes, labelled MP in the figure. Contours were determined using the Kamb method (Robin and Jowett, 1986) and are given in multiples of the density expected for a uniform distribution starting with 1 and increasing with increments of 0.67.

As discussed above, an orthorhombic fabric is not sufficient in itself to deduce the slip vector for a fault zone; any of the three mirror planes could coincide with the mirror plane of the deformation. This ambiguity is resolved if we consider the Riedel structures and folds together as subfabrics of the total fault-zone fabric. According to Paterson and Weiss (1961), only those symmetry elements common to all the subfabrics are elements of the total fabric. Comparing figures 16B and 18B, only one mirror plane is common to both subfabrics, so that the total fabric has monoclinic symmetry. We conclude that this mirror plane contains the slip vector, which would be top-to-the-southwest.

We interpret the origin and geometry of the Riedel structures as follows. The structures formed in response to slip in local brittle shear zones, the orientation of which is recorded by Y structures (fig. 21). Gapais and others (1987) discussed general relationships among patterns of localized shear zones on the one hand and the bulk strain and strain history of the deformed rocks containing the zones on the other. They proposed a correlation between the symmetry of shear-zone patterns and the "degree of non-coaxiality of bulk deformation history" (p. 636) and stated that the orthorhombic symmetry of conjugate, symmetric sets of shear zones is indicative of coaxial histories. Accordingly, we hypothesize that the opposing sense of slip on each group of Y-structures in the Rosario zone resulted in bulk shortening of the zone normal to its bounding faults (fig. 21) and possibly in extension parallel to its strike. On the basis of the monoclinic symmetry of the combined sub-fabrics, we suggest that this fault-normal shortening was part of the overall progressive deformation that also resulted in the Rosario folds: a general shear combining top-to-the-southwest slip and northeast-southwest fault-normal shortening. An alternative interpretation is that the shear zones developed during a coaxial phase of deformation subsequent to the non-coaxial shear responsible for the folds. In this case, the two deformations might have coincidentally shared a common symmetry element, the northeast-striking mirror plane.

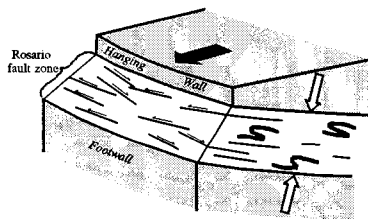


Fig. 21. Schematic illustration of structures in the Rosario fault zone, as viewed from the south. The inferred general shear comprised: (A) top-to-the-southwest slip (large solid arrow), responsible for forming the asymmetric folds; and (2) shortening normal to the fault zone (two large open arrows), responsible for forming two groups of obliquely inclined but symmetric brittle shear zones containing Riedel structures. Each of these groups had an opposing sense of slip (small arrows) with an average slip direction oriented approximately parallel to the strike of the fault zone.

GEOMETRY AND TIMING OF DEFORMATION IN THE SAN JUAN ISLANDS

On the basis of our analysis, we propose that: (1) the average direction of slip for the Lopez fault zone was top-to-the-south; (2) the average slip direction for the Rosario fault zone was top-to-the-southwest; and (3) in the Rosario zone, the general non-coaxial deformation responsible for the asymmetric folds also resulted in northeast-southwest, fault-normal shortening accommodated on two groups of oblique shear zones with local, sub-horizontal slip directions of top-to-the-northwest and top-to-the-southeast, respectively.

On the following grounds, we propose that these structures are geometrically and temporally related. First, as discussed above, the structures used for the kinematic analysis are developed in mesoscopically ductile cataclastic fault rocks. Field and petrographic evidence from the Rosario and Lopez fault zones (see also Brandon, Cowan, and Feehan, 1993; Brandon, Cowan, and Vance, 1988) shows that cataclastic deformation preceded the static, high-pressure, low-temperature metamorphism that affected fault rocks and nappes alike throughout the archipelago. Second, fault rocks, blocks, and lenses in both zones are locally (Rosario) to pervasively (Lopez) overprinted by the penetrative solution-mass-transfer cleavage. We reviewed above the geologic and geochronologic evidence supporting the interpretation that kilometer-scale slip on the faults, metamorphism, and the development of cleavage all occurred between 100 and about 84 Ma. These controls on timing collectively establish the general temporal relationship of the mesoscale structures analyzed in this study. Given the fact that faulting was the earliest event in the orogenic history, only a fraction of the 16 my interval was available for formation of fault structures.

Regarding the geometry of deformation, the slip vectors based on mesoscale folds indicate a general top-to-the-southwest slip direction. If the slip vectors determined from Riedel structures record thinning of the Rosario fault zone, the geometry of this deformation is compatible with the average transport direction of the nappes constituting the upper plates of the Lopez and Rosario faults. Finally, the solution-mass-transfer cleavage in the southern San Juan Islands has an average northwest strike and northeast dip. Its attitude approximates the average attitude of the Lopez and Rosario fault zones, but the cleavage dips about 20° more steeply. The pole to cleavage provides an approximation for the maximum shortening direction during cleavage formation and indicates that orogenic shortening during this phase of deformation also was oriented northeast-southwest.

SUMMARY AND CONCLUSIONS

1. We present a statistical method for synoptic analysis of mesoscale structures in brittle fault zones. In this method, we determine the mean orientation of the distribution of internal rotation axes representing asymmetric folds and Riedel structures in the fault zone and then establish the symmetry of the orientation distribution. A critical test is

whether the symmetry of the distribution is compatible with the monoclinic symmetry of an idealized two-dimensional shear zone. If so, we use the mean direction of the distribution, together with the shear sense of the component structures, to define a mirror plane and slip vector.

2. For the Lopez and Rosario folds, internal rotation axes are subparallel to the shear plane and are moderately to widely dispersed within it. The distribution is Gaussian and centered around the synoptic internal rotation axis. We hypothesize that this random variation about a mean direction is due to stochastic processes associated with faulting and to antecedent processes that produced structures in the rock prior to faulting. These processes may include local perturbations in the orientation of the slip direction with respect to layering and shear planes or rotations of mesoscale domains about fault-normal axes.

3. We propose that the internal rotation axes associated with individual Riedel structures are also amenable to a synoptic, symmetry-based analysis. In contrast to the two fold datasets, the Riedel structures from the Rosario fault zone show a symmetric bimodal distribution of internal rotation axes, which we attribute to slip on two oblique set of shear zones. The Riedel structures evidently record thinning of the fault zone concomitant with the top-to-the-southwest slip across it.

4. Our results reinforce the conclusions of Hansen (1967, 1971), Woodcock (1979), Rutter and others (1986), and Chester and Logan (1987): in brittle fault and shear zones dominated by microfracturing and cataclastic flow, kinematically useful mesoscale structures, such as asymmetric folds and Riedel structures, must be analyzed synoptically. Interpretations of regional sense-of-shear using small datasets are liable to be incorrect and could yield a result in error by as much as 180°, because of the extreme variability in the orientation of individual component structures.

5. Our conclusion of southwest-directed Late-Cretaceous transport in the San Juan Islands is consistent with the contraction model of Brandon and Cowan (1985) and McGroder (1991), which holds that the entire Cretaceous orogen developed during regional southwest-northeast shortening, probably in response to the collision of the Insular superterrane with North America. Other indications of southwest-northeast shortening include: (A) the trend of the Late Cretaceous Nanaimo basin, which is interpreted to have formed as a flexural fore-deep in front of the thrust belt (fig. 3A); (B) the trend of the high-temperature metamorphic core of the Cascades, which marks the locus of greatest crustal thickening within the orogen (Miller and others, 1993); and (C) the northeast transport directions of several coeval mid-Cretaceous thrust sheets in the eastern Cascade foldbelt (McGroder, 1989). Our results are at variance with the transcurrent model of Brown (1987), Smith (1988), and Maekawa and Brown (1991), which calls for top-to-the-north-northwest slip in a dominantly transcurrent setting.

ACKNOWLEDGMENTS

Our field work in the San Juan Islands was supported from 1976 to 1985 by the National Science Foundation. We also acknowledge NSF grants EAR-9005777 (Brandon) and EAR-9218402 (Cowan). We have benefited from discussions with Jeff Feehan, Win Means, Gian Andrea Pini, Jan Tullis, and Steve Wojtal. Detailed and helpful reviews by Rick Allmendinger, Win Means, Rich Schweickert, Rolfe Stanley, and Rob Twiss helped us to clarify our presentation.

REFERENCES

- Angelier, J., 1984. Tectonic analysis of fault slip data sets: *Journal of Geophysical Research*, v. 89, p. 5835–5848.
- Babcock, R. S., and Misch, P., 1988. Evolution of the crystalline core of the North Cascades Range. *In* Ernst, W. G., ed., *Metamorphism and crustal evolution of the western United States*: Englewood Cliffs, Prentice-Hall, p. 214–232.
- Bell, T., 1978. Progressive deformation and reorientation of fold axes in a ductile mylonite zone: the Woodroffe thrust: *Tectonophysics*, v. 44, p. 285–320.
- Berthé, D., Choukroune, P., and Jegouzo, P., 1979. Orthogneiss, mylonite and non-coaxial deformation of granites: the example of the South Armorican Shear Zone: *Journal of Structural Geology*, v. 1, p. 31–42.
- Brandon, M. T., ms, 1980. Structural geology of middle Cretaceous thrust faulting on southern San Juan Island, Washington. M.S. thesis, University of Washington, Seattle, 130 p.
- _____, 1989. Geology of the San Juan-Cascade nappes, northwestern Cascade Range and San Juan Islands. *In* Joseph, N. L., and others, editors, *Geologic Guidebook for Washington and Adjacent Areas*: Washington Division of Geology and Earth Resources Information Circular 86, p. 137–162.
- Brandon, M. T., and Cowan, D. S., 1985. The Late Cretaceous San Juan Islands-northwestern Cascades thrust system: *Geological Society of America Abstracts with Programs*, v. 17, p. 343.
- Brandon, M. T., Cowan, D. S., and Feehan, J., 1993. Discussion of, "Kinematic analysis of the San Juan thrust system, Washington" by H. Maekawa and E. H. Brown: *Geological Society of America Bulletin*, v. 105, p. 839–841.
- Brandon, M. T., Cowan, D. S., and Vance, J. A., 1988. The Late Cretaceous San Juan thrust system, San Juan Islands, Washington: *Geological Society of America Special Paper* 221, 81 p.
- Brown, E. H., 1987. Structural geology and accretionary history of the Northwest Cascades system, Washington and British Columbia: *Geological Society of America Bulletin*, v. 99, p. 201–214.
- Brown, E. H., and Talbot, J. L., 1989. Orogen-parallel extension in the North Cascades crystalline core: *Tectonics*, v. 8, p. 1105–1114.
- Carreras, J., and Santanach, P. F., 1973. Micropliegues y movimiento en los cizallamientos profundos del Cabo de Creus: *Estudios Geológicos*, v. 29, p. 439–450.
- Carroll, P. R., 1980. Petrology and structure of the pre-Tertiary rocks of Lummi and Eliza Island, Washington: M.S. thesis: University of Washington, Seattle, 78 p.
- Chester, F. M., Friedman, M., and Logan, J. M., 1985. Foliated cataclases: *Tectonophysics*, v. 111, p. 139–146.
- Chester, F. M., and Logan, J. M., 1987. Composite planar fabric of gouge from the Punchbowl Fault, California: *Journal of Structural Geology*, v. 9, p. 621–634.
- Coney, P. J., 1974. Structural analysis of the Snake Range "Décollement," east-central Nevada: *Geological Society of America Bulletin*, v. 85, p. 973–978.
- Davis, J. C., 1986. *Statistics and data analysis in geology*: New York, John Wiley & Sons, second edition, 646 p.
- Davis, G. A., Monger, J. W. H., and Burchfiel, B. C., 1978. Mesozoic construction of the Cordilleran "collage," central British Columbia to central California. *In* Howell, D. G., and McDougall, K. A., editors, *Mesozoic Paleogeography of the Western United States*: Society of Economic Paleontologists and Mineralogists, Pacific Section, p. 1–32.
- England, T. D. J., and Calon, T. J., The Cowichan fold and thrust system, Vancouver Island, Southwestern British Columbia: *Geological Society of America Bulletin*, v. 103, p. 336–362.
- Gapais, D., Bale, P., Choukroune, P., Cobbold, P. R., Mahjoub, Y., and Marquer, D., 1987. Bulk kinematics from shear zone patterns: some field examples: *Journal of Structural Geology*, v. 9, p. 635–646.

- Carver, J. I., 1988, Stratigraphy, depositional setting, and tectonic significance of the clastic cover to the Fidalgo Ophiolite, San Juan Islands, Washington: *Canadian Journal of Earth Sciences*, v. 25, p. 417–432.
- Hancock, P. L., 1985, Brittle microtectonics: principles and practice: *Journal of Structural Geology*, v. 7, p. 437–457.
- Hanmer, S., and Passchier, C., 1991, Shear-sense indicators: a review: *Geological Survey of Canada, Paper 90-17*, 72 p.
- Hansen, Edward, 1967, Methods of deducing slip-line orientations from the geometry of folds: *Carnegie Institution of Washington Yearbook*, v. 65, p. 387–405.
- , 1971, *Strain Facies*: New York, Springer-Verlag, 207 p.
- Haugerud, R. A., van der Heyden, P., Tabor, R. W., Stacey, J. S., and Zartman, R. E., 1991, Late Cretaceous and early Tertiary plutonism and deformation in the Skagit Gneiss Complex, North Cascade Range, Washington and British Columbia: *Geological Society of America Bulletin*, v. 103, p. 1297–1307.
- Johnson, S. Y., Zimmerman, R. A., Naeser, C. W., and Whetten, J. T., 1986, Fission-track dating of the tectonic development of the San Juan Islands, Washington: *Canadian Journal of Earth Sciences*, v. 23, p. 1318–1330.
- Journeay, J. M., and Friedman, R. M., 1993, The Coast Belt Thrust System: Evidence of Late Cretaceous shortening in southwest British Columbia: *Tectonics*, v. 12, p. 756–775.
- Kamb, W. B., 1959, Ice petrofabric observations from Blue Glacier, Washington, in relation to theory and experiment: *Journal of Geophysical Research*, 64, p. 1891–1909.
- Kano, K., Nakaji, M., Takeuchi, S., 1991, Asymmetrical melange fabrics as possible indicators of the convergent direction of plates: a case study from the Shimanto Belt of the Akaishi Mountains, central Japan: *Tectonophysics*, v. 185, p. 375–388.
- Krantz, R. W., 1988, Multiple fault sets and three-dimensional strain: theory and application: *Journal of Structural Geology*, v. 10, p. 225–237.
- Lister, G. S., and Williams, P. F., 1983, The partitioning of deformation in flowing rock masses: *Tectonophysics*, v. 92, p. 1–33.
- Logan, J. M., Friedman, M., Higgs, N., Dengo, C., and Shimamoto, T., 1979, Experimental studies of simulated gouge and their application to studies of natural fault zones, in *Proceedings of Conference VIII on Analysis of Actual Fault Zones in Bedrock*: U.S. Geological Survey Open-File Report 79-1239, p. 305–343.
- Maekawa, H., and Brown, E. H., 1991, Kinematic analysis of the San Juan thrust system, Washington: *Geological Society of America Bulletin*, v. 103, p. 1007–1016.
- , 1993, Reply to discussion of "Kinematic analysis of the San Juan thrust system, Washington": *Geological Society of America Bulletin*, v. 105, p. 841–844.
- Malavieille, J., 1987, Extensional shearing deformation and kilometer-scale "a"-type folds in a Cordilleran metamorphic core complex (Raft River Mountains, northwestern Utah): *Tectonics*, v. 6, p. 423–448.
- Mardia, K. V., 1972, *Statistics of directional data*. London, Academic Press, 357 p.
- Marrett, R., and Allmendinger, R. W., 1990, Kinematic analysis of fault-slip data: *Journal of Structural Geology*, v. 12, p. 973–986.
- McGroder, M. F., 1989, Structural geometry and kinematic evolution of eastern Cascades foldbelt, Washington and British Columbia: *Canadian Journal of Earth Sciences*, v. 26, p. 1586–1602.
- , 1991, Reconciliation of two-sided thrusting, burial metamorphism, and diachronous uplift in the Cascades of Washington and British Columbia: *Geological Society of America Bulletin*, v. 103, p. 189–209.
- Means, W. D., Hobbs, B. E., Lister, G. S., and Williams, P. F., 1980, Vorticity and non-coaxiality in progressive deformation: *Journal of Structural Geology*, v. 2, p. 371–378.
- Miller, R. B., Brown, E. H., McShane, D. P., and Whitney, D. L., 1993, Intra-arc crustal loading and its tectonic implications, North Cascades crystalline core, Washington and British Columbia: *Geology*, v. 21, p. 255–258.
- Misch, P., 1966, Tectonic evolution of the Northern Cascades of Washington State—a west-Cordilleran case history: *Canadian Institute of Mining and Metallurgy, special volume 8*, p. 101–148.
- , 1977, Dextral displacements at some major strike faults in the North Cascades: *Geological Association of Canada, Programs with Abstracts*, v. 2, p. 37.
- Monger, J. W. H., 1986, Geology between Harrison Lake and Fraser River, Hope map area, southwestern British Columbia: *Geological Survey of Canada Paper 86-1B*, p. 699–706.
- , 1990, Georgia Basin: Regional setting and adjacent Coast Mountains geology, British Columbia: *Geological Survey of Canada, Paper 90-1F*, p. 95–107.
- Monger, J. W. H., Price, R. A., and Tempelman-Kluit, D. J., 1982, Tectonic accretion and the origin of the two major metamorphic and plutonic belts in the Canadian Cordillera: *Geology*, v. 10, p. 70–75.

- Moore, J. C., and Wheeler, R. L., 1978, Structural fabric of a mélange, Kodiak Islands, Alaska: *American Journal of Science*, v. 278, p. 739–765.
- Morgenstern, N. R., and Tchalenko, J. S., 1967, Microscopic structures in kaolin subjected to direct shear: *Geotechnique*, v. 17, p. 309–328.
- Nye, J. F., 1985, *Physical properties of crystals*: Oxford, England, Clarendon Press, 329 p.
- Palumbo, G. T. X., and Brandon, M. T., 1990, Gravity modeling of the geometry of the frontal thrust to the Late Cretaceous San Juan nappes, NW Washington State: *Geological Society of America, Abstracts with Programs*, v. 22, p. A325.
- Paterson, M. S., and Weiss, L. E., 1961, Symmetry concepts in the structural analysis of deformed rocks: *Geological Society of America Bulletin*, v. 72, p. 841–882.
- Petit, J. P., 1987, Criteria for the sense of movement on fault surfaces in brittle rocks: *Journal of Structural Geology*, v. 9, p. 597–608.
- Platt, J. P., Leggett, J. K., and Alam, S., 1988, Slip vectors and fault mechanics in the Makran accretionary wedge, southwest Pakistan: *Journal of Geophysical Research*, v. 93, p. 7955–7973.
- Press, W. H., Flannery, B. P., Teukolsky, S. A., and Vetterling, W. T., 1986, *Numerical recipes*: Cambridge, England, Cambridge University Press, 818 p.
- Robin, P.-Y. F., and Jowett, E. C., 1986, Computerized density contouring and statistical evaluation of orientation data using counting circles and continuous weighting functions: *Tectonophysics*, 121, p. 207–223.
- Rubin, C. M., Saleeby, J., Cowan, D. S., Brandon, M. T., and McGroder, M. F., 1990, Regionally extensive mid-Cretaceous west-vergent thrust system in the northwestern Cordillera: Implications for continent-margin tectonism: *Geology*, v. 18, p. 276–280.
- Rutter, E. H., Maddock, R. H., Hall, S. H., and White, S. H., 1986, Comparative microstructures of natural and experimentally produced clay-bearing fault gouges: *Pure and Applied Geophysics*, v. 124, p. 3–30.
- Sanderson, D., 1973, The development of fold axes oblique to the regional trend: *Tectonophysics*, v. 16, p. 55–70.
- Smith, M., 1988, Deformational geometry and tectonic significance of a portion of the Chilliwack Group, northwestern Cascades, Washington: *Canadian Journal of Earth Sciences*, v. 25, p. 433–441.
- Stanley, R. S., and Sarkisian, A., 1972, Analysis and chronology of structures along the Champlain thrust west of the Hinesburg synclinorium, in Doolan, B., and Stanley, R. S., eds., *Guidebook for Field Trips in Vermont*: Burlington, Vermont, University of Vermont, Department of Geology, p. 117–150.
- Suppe, J., 1985, *Principles of Structural Geology*: Englewood Cliffs, Prentice-Hall, Inc., 537 p.
- Taira, A., Byrne, T., and Ashi, J., 1992, *Photographic Atlas of an Accretionary Prism. Geologic Structures of the Shimanto Belt, Japan*: Tokyo, Japan, University of Tokyo Press, 124 p.
- Tanaka, H., 1992, Cataclastic lineations: *Journal of Structural Geology*, v. 14, p. 1239–1252.
- Tchalenko, J. S., 1968, The evolution of kink-bands and the development of compression textures in sheared clays: *Tectonophysics*, v. 6, p. 159–174.
- Twiss, R. J., and Gefell, N. J., 1990, Curved slickenfibers: a new brittle shear sense indicator with application to a sheared serpentinite: *Journal of Structural Geology*, v. 12, p. 471–481.
- Twiss, R. J., Protzman, G. M., and Hurst, S. D., 1991, Theory of slickenline patterns based on the velocity gradient tensor and microrotation: *Tectonophysics*, v. 186, p. 215–239.
- Wheeler, R. L., 1978, Slip planes from Devonian Millboro Shale, Appalachian Plateau Province: Statistical extensions of disclod analysis: *American Journal of Science*, v. 278, p. 297–517.
- Woodcock, N. H., 1979, The use of slump structures as paleoslope orientation estimators: *Sedimentology*, v. 26, p. 83–99.